Evidence for crustal removal, tectonic erosion and flare-ups from the Japanese evolving forearc sediment provenance

Daniel Pastor-Galán[1,2,3], Christopher J. Spencer[4,5], Tan Furukawa[3], Tatsuki Tsujimori[2,3]

[1]Frontier Research Institute for Interdisciplinary Science, Tohoku University, Japan

[2]Center for North East Asian Studies, Tohoku University, 980-8576, 41 Kawauchi, Aoba-ku, Sendai, Miyagi, Japan

[3]Department Earth Science, Tohoku University, Japan

[4]School of Earth and Planetary Sciences, The Institute for Geoscience Research (TIGeR), Curtin University, Perth, Australia

[5]Department of Geological Sciences and Geological Engineering, Queen's University, Kingston, Canada

Abstract

Forearc basins preserve the geologic record relating strictly to arc magmatism. The provenance of forearc sediment can be used to differentiate periods of crustal growth, accretion, and destruction, enhanced magmatism, advancing and retreating subduction slabs, delamination, etc. All these tectonic events systems predict differing degrees of sedimentary reworking of the older forearc units. Additionally, Hf isotopes of zircon can be used to evaluate the degree of continental reworking that occurs in the arc system. In this paper, we evaluate the changes in a long-lived subduction system using detrital zircon U-Pb and Hf data from forearc units in northern Honshu, Japan that span in age from the Silurian Period to the present from the forearc provenance of the Japanese subduction system. Our data demonstrate a series of dominant age peaks (430 ± 20, 360 ± 10, 270 ± 20, 184 ± 12, 112 ± 22, and 7 ± 7 Ma) and a progressive loss of the older zircon populations. Zircon Hf data reveal three discrete shifts that correspond to differing degrees of isotopic enrichment and correlate with changes in the dominant zircon age peaks. Additionally, each temporal isotopic shift is associated with isolation of the older sedimentary packages wherein no detrital zircon from the previous stages are observed in subsequent stages. We propose these shifts provide evidence for rapid shifts in arc tectonics including: magmatic flare-ups, producing the dominant peaks; protracted tectonic erosion progressively removing older sources of zircons reveals; a late Carboniferous event triggering the complete removal of the Precambrian crust; and the Cretaceous melting of the entire Permian arc crust, likely related with the subduction of the mid-oceanic ridge separating the Izanagi and Pacific plates.

Keywords:

Detrital zircon, geochronology, Lu-Hf, crustal growth, tectonic erosion

Highlights

-We identified six magmatic flare-ups from Silurian to present day in the N Honshu arc

- N Honshu underwent a protracted history of tectonic erosion

-Late Carboniferous delamination substituted the Precambrian crust for a brand new one

-Late Carboniferous crust melted in the Cretaceous after the Izanagi ridge subduction

1. Introduction

The history of the Earth, since the Archean, is carved in the continent's crustal record: the earliest rocks differentiated from the mantle; the origin, evolution of life; the evolution of the magnetic field or the development of superplumes from the core-mantle boundary. Unfortunately, this information is disrupted and fragmented, the crust not only grows but recycles back into the mantle by a variety of processes. The continental crust grows by magmatism in arcs (e.g. Spencer et al., 2017), whereas it gets destroyed primarily in subduction zones through subduction of sediments, tectonic erosion (a.k.a. subduction erosion, von Huene and Lallemand, 1990), and lithospheric delamination s.l. (e.g. Magni and Kiraly, 2019). Tectonic erosion is the removal of upper-plate material from the forearc at convergent margins, originally proposed in the Japan and Peru Trenches by von Huene and Lallemand (1990). The global budget of continental crust has not been always neutral and there have been episodes of net growth and shrink (e.g. Spencer et al., 2019). Interestingly, during the episodes of net growth parts of the crust may have been vigorously destroyed and vice versa. Documenting the origin and fate of the continental crust is a key goal of the Earth sciences to understanding Earth's chemical evolution and the main tectonic processes operating through time. Sialic crustal growth and destruction are, in addition, crucial to develop accurate plate restorations and paleogeography, which in turn are the foundation of Earth history, paleoclimatic studies, and tectonic research. Without accurate constraints of when and where a piece of crust existed such reconstructions are useless for their primary purpose.

The Panthalassa–Pacific ocean system has been subducting below today's East Asia–Oceania for at least 500 m.yrs (e.g. Maruyama and Seno, 1986; Isozaki et al., 2010). The consumption of this superocean formed two of the largest accretionary orogens of the Phanerozoic where the continental crust grew significantly from ~1000 to 250 Ma in the Central Asian Orogenic Belt (Jahn et al., 2004) and ~800 to 250 Ma in the Terra Australis Orogen (Cawood, 2005). In contrast, the Japan arc is a narrow strip with a cyclic record fragmented accretionary complexes and blueschist (s.l.) exhumation during ~500 m. yr. of subduction preserved over a Cretaceous granitic crust. Although tectonic erosion has played an important role in the poor preservation of the Japanese basement (e.g. Isozaki et al., 2010), this process has been apparently common in growing orogens (e.g. Stern, 2011). The reasons why the Japan arc behaved so differently to its counterparts in the Panthalassa–Pacific subduction zone are poorly known due to the discontinuity, large gaps, and scarcity of its crustal record.

Forearc basins preserve the geologic record relating strictly to arc magmatism where the bulk of the continental crust is created and destroyed. Although sediment from the volcanic arc is transported both to the backarc and forearc regions, the forearc is less likely to receive detritus from the hinterland as the magmatic arc often forms a continental divide. In this study, we investigate the crustal evolution of the northern Honshu arc (NE Japan) from the Silurian to the present day through the provenance of detrital zircons and their Hf signature in the South Kitakami forearc basin, which contains a close to continuous sedimentary record (cf. Ehiro et al., 2016). Our new results, together with a reappraisal of former studies, show a fierce history of periodic flare-ups, tectonic erosion, complete removal of the Precambrian crust in the late Carboniferous, and total melting of the Permian crust in the Cretaceous.

2. Geological Background

The Japanese archipelago is a 3000 km long bow-shaped chain of islands along the eastern margin of Asia preserving at least 500-million-year history of subduction processes (e.g. Maruyama et al., 1997; Isozaki et al., 2010). At present, it is located at the junctions of four distinct plates Eurasian, Pacific, North American, and Philippine Sea plates (Fig. 1). The Pacific plate is subducting at a rate of 10 cm/yr beneath NE Japan, whereas the Philippine Sea plate is subducting from SE to NW with 4 cm/yr under SW Japan along the Nankai trough (trench) and Ryukyu trench off SW Japan.

2.1 Geological history of Japan

The origins of the present-day archipelago are tied to the breakup of the supercontinent Rodinia (e.g. Maruyama et al., 1997; Pastor-Galán et al., 2019), in particular to both North and South China cratons that rifted apart from Rodinia while Panthalassa ocean (paleo-Pacific) opened (e.g. Isozaki et al., 2010).

After an uncertain period of Precambrian evolution, an ocean (perhaps the Panthalassa) commenced subduction below what today is Japan arc. The oldest subduction-related rocks in both NW and SW Japan arcs are late Cambrian arc-type granitoids, serpentinized mantle wedge peridotites with jadeitites (e.g., Isozaki et al., 2015; Tsujimori, 2017). Despite their paucity and dismembered nature, they indicate the subduction history of Japan commenced at least ~500 Ma. It has been postulated that the proto-Japan arc formed part of eastern Cathaysia passive margin (Fig. 1) from late Proterozoic to early Paleozoic until subduction initiated or flipped in polarity during late Cambrian. This hypothesis is grounded on the fact that the majority of the Paleozoic stratigraphy of Japan suggest a connection with Cathaysia (e.g. Isozaki et al., 2010; Isozaki 2019; Wakita et al., 2021). Some authors suggested, however, that that areas of Japan (e.g. Hitachi, Akiyoshi, Ultra-Tamba) show robust coincidences with North China Craton and at least parts of Japan may have originated there (Tagiri et al., 2011; Wakita et al., 2021). Finally, some researchers think that the Japanese crust could be a fragment from NE Gondwana that migrated northwards together with the opening of the Neotethys during the Permian as an oceanic island arc to finally collide with both North and South China (Otoh et al., 1990; Okawa et al., 2013)

From late Ordovician, the same subduction regime apparently continued until today, firstly as a continental arc to finally develop a small-scale back-arc basin with minimal formation of true oceanic crust (Japan Sea) during the Miocene (e.g. Maruyama et al., 1997). The only continent-continent collision record in Japan is found in the Hida Belt, an allochthonous unit thrusted over pre-Jurassic units during the Triassic collisional orogeny that sutured North and South China cratons (e.g. Isozaki, 1997; Ernst et al., 2007; Fig. 1). The absence of evidence for other collisional events supports a Panthalassa-Pacific facing arc from the Ordovician attached to the South China margin (e.g. Isozaki et al., 2014) rather than a Gondwana derived Tethyan facing arc colliding against China (Okawa et al., 2013).

The geotectonic units of present day Japan archipelago are divided into SW and NE Japan by the Tanakura Tectonic line (Fig. 1). SW Japan is characterized by a series of orogen-parallel accretionary complexes; the Median Tectonic Line further separate the inner and outer zones. The overall structure is a pile of north-rooting, subhorizontal nappes, which older sheets usually occupy the upper structural positions. Voluminous calc-alkaline granitic batholiths and low-pressure/high-temperature (LP-HT) metamorphic rocks intruded the nappe structure in Cretaceous time, gently folding them to form synform-antiform structures. This magmatic event has been interpreted as a flare-up caused by the subduction of a mid ocean ridge (Maruyama and Seno, 1986). In contrast, the nappe distribution in NE Japan is geometrically more complex due to significant structural complications (Fig. 2) together with a thick cover of Cenozoic volcanic rocks and sediments. Exposures of pre-Jurassic geotectonic units and Cretaceous batholiths in NE Japan are limited mainly in the Kitakami and Abukuma Mountains. Although the subhorizontal nappe-pile structure is completely disrupted by a N-S tending high angle faults, all lithological component in NE Japan can be comparable to those in SW Japan (e.g., Isozaki et al., 2010).

In the ~500 m.yrs orogenic history (Fig. 1), the processes of accretion have been, apparently, episodic at Carboniferous; Late Permian, which included the collision of an oceanic arc; Jurassic; and Late Cretaceous to the present (e.g. Isozaki et al., 2010). Several fragments of serpentinized mantle wedge peridotites/serpentinites and intra-oceanic crust–mantle successions have been described: ~540 Ma (Oeyama and Miyamori–Hayachine), ~280 Ma (Yakuno), Late Jurassic (Mikabu and Horokanai), Late Cretaceous (Poroshiri) and Cretaceous-Eocene crystallization ages (Mineoka) (e.g., Ishiwatari and Tsujimori, 2003). In addition to these rocks, three high-pressure/low-temperature (HP-LT) metamorphic belts crop-out with ages of 360–300 Ma (Renge), 240–200 Ma (Suo), and 120–60 Ma (Sanbagawa and Kamuikotan) (Tsujimori and Itaya, 1999). Notably the Renge and the equivalents HP-LT rocks occurs in the serpentinite mélange associated with the Oeyama and Miyamori–Hayachine units, and 120–60 Ma HP-LT rocks in the inner zone of SW Japan are well paired with granitic batholiths and LP-HT metamorphic rocks in the inner zone (Miyashiro, 1961; Fig. 1).

A very particular feature of the present-day arc crust in Japan is that it is mostly Cretaceous or younger. Crustal-scale seismic cross-section of SW Japan reveled pre-Cretaceous rocks occur as roof pendant at shallow depths (e.g. Ito et al., 2009). Despite the 400 m.yrs of pre-Cretaceous subduction history, pre-Cretaceous plutonic rocks are very scarce. Exposure of ~500–400 Ma granites are limited as fragments in the Kurosegawa Belt that is a klippe-like narrow composite unit in the outer zone of SW Japan and fault-bounded small blocks of the Kitakami Mountains of NE Japan (e.g. Isozaki et al., 2015; Shimojo et al., 2010). The best exposure of these granitic bodies is the Hikami Granite (Fig. 2 and SF-1) formed ~450–440 Ma (e.g. Shimojo et al., 2010; Isozaki et al., 2015). The ~300 Ma granites are extremely rare, and ~250–200 Ma granitoids only occur within the Hida Belt in central Japan. Several authors, primarily based on detrital zircon U-Pb ages studies, speculated that the pre-existing older arc crusts had been significantly removed, probably subducted into the mantle, by multiple episodes of tectonic erosion (e.g. Isokaki et al., 2010; Suzuki et al., 2010; Aoki et al., 2012). This secondary disappearance of older crust contributed to the shortage of information for paleogeographic reconstruction of Paleozoic and older Japan.

2.2 Geology of the South Kitakami Mountains

The South Kitakami Mountains (SKM hereafter) lie in Tohoku (NE Honshu, Fig. 2) and is the only relatively thick Paleozoic and Mesozoic continental margin forearc basin in Japan. SKM also contains the some of the scarce Cambrian-Silurian arc granitoids (Isozaki et al., 2015), a weakly metamorphosed accretionary complex (the Motai metamorphic rocks, locally blueschist-facies), which has been compared to the Renge HP-LT metamorphic rocks of the SW Japan (Tsujimori and Itaya, 1999), and a supra-subduction zone ophiolite (Hayachine–Miyamori Complex: Ozawa et al., 2015) (cf. Ehiro et al., 2016). The South Kitakami forearc basin (SKFB hereafter) represent an independent tectonostratigraphic unit that contains a nearly continuous forearc basin sequence from Silurian to Early Cretaceous that lies conformably over the Hikami granite and in tectonic contact with the accretionary and metamorphic units.

The SKFB comprises unmetamorphosed shallow-marine Silurian to Early Cretaceous strata (Fig. 1). The succession (Ehiro et al., 2016 and references therein) starts with a basal arkose overlain by Silurian limestone and tuff to Devonian tuff and interlayered mud- and sandstone. Then those are unconformably overlain by the Early Carboniferous interlayered mud- and sandstone with some tuffaceous rocks followed by massive late Carboniferous limestones. Over a minor unconformity Permian shallow marine clastic strata with volcaniclastics, limestones, and conglomeratic intercalations occur. The Mesozoic strata (Triassic to lowest Cretaceous) are located in the southern part of the SKM and were deposited in a shallow marine or alluvial environment and are mainly composed of clastic rocks in association with rare limestone and tuff. The Mesozoic stratigraphy starts over a disconformity with the Paleozoic strata and contains several minor unconformities (Fig. 2). This succession ends with a thick volcanic sequence at the Lower Cretaceous (Ehiro et al., 2016) and was heavily intruded during the Aptian-Albian (Fig. 1; e.g. Tsuchiya et al., 2014; Osozawa et al., 2019). The Aptian-Albian Cretaceous granitoids of the SKM show frequently adakitic or shoshonitic composition and ages ranging from 127–113 Ma (e.g. Osozawa et al., 2019; SF-1). These plutons are slightly older than the equivalent Cretaceous granitoids exposed in SW Japan.

Previous detrital zircon studies in the SKM (Shimojo et al., 2010; Okawa et al., 2013; Isozaki et al., 2014) tried to unravel the enigmatic pre-Mesozoic paleogeography of Japan in an attempt to link sediment provenance with contrasting results. The studies found a paucity of Precambrian zircons, which corroborates the forearc setting, where little support from the continent is expected, but in turn prevents paleogeographic correlations. Okawa (2013) suggested the affinity of SKM with Gondwana. In contrast, Isozaki et al. (2014, 2015) emphasized similarities of SKM, SW Japan and E Russia with the South China block, supporting the hypothesis of a 'Greater South China Craton'.

3. Sampling, Methods, and Results

Fourteen fore-arc sedimentary clastic samples with ages from Silurian to present-day and one igneous sample (Hikami pluton, late Ordovician–early Silurian) were collected from the SKM of NE Honshu (Samples coded Kita; Fig. 2, Supplementary File SF-1). Biostratigraphic constraints demonstrate the age of sedimentary units spanning from the Silurian Period to the present (Fig. 2 and SF-1 for in detail rock formation). Zircon extraction followed traditional mineral separation techniques (crushing, milling, sieving, Wilfley table, Franz magnetic separation, and heavy liquid separation). Zircon were mounted in epoxy, imaged with cathodoluminescence, and analyzed for U-Pb and Hf during two sessions via laser ablation inductively coupled plasma mass spectrometry (LA-ICP-MS) in the John de Laeter Centre (JdLC) at Curtin University with a Resonetics RESOlution M-50A-LR, incorporating a Compex 102 excimer laser. Following a 15–20 s period of background analysis, samples were spot ablated for 30 s at a 7 Hz repetition rate using a 33 μm beam and laser energy of 1.7 J/cm2 at the sample surface. The sample cell was flushed by ultrahigh purity He (0.68 L min−1) and N2 (2.8 mL min−1). Isotopic intensities were measured using an Agilent 7700s quadrupole ICP-MS and a Nu Instruments Plasma II MC-ICP-MS, with high purity Ar as the plasma gas (flow rate 0.98 L min−1). On the quadrupole, most elements were monitored for 0.01 s each with the exception of ^{88}Sr (0.02 s), ^{139}La (0.04 s), ^{141}Pr (0.04 s), ^{204}Pb, ^{206}Pb, ^{207}Pb, ^{208}Pb (all Pb 0.03 s), ^{232}Th (0.0125 s), and ^{238}U (0.0125 s). Approximately half of the split was sent to a Nu Plasma II MC-ICP-MS for Lu–Hf isotopic measurement. Masses for ^{172}Yb, ^{173}Yb, ^{175}Lu, ^{176}Hf + Yb + Lu, ^{177}Hf, ^{178}Hf, ^{179}Hf, and ^{180}Hf were measured simultaneously. Concordant zircon ages were defined as those for which the calculated ages from two U–Pb systems lie within uncertainty of one another (Spencer et al., 2016). Propagated uncertainties larger than 10% were considered unreasonable and these data were excluded. εHf(t) values were calculated for all data using the ^{176}Lu decay constant = 1.865 x 10−11 year−1 (Scherer et al., 2001). Chondritic values are after Bouvier et al. (2008); ^{176}Hf/^{177}Hf CHUR = 0.282785, ^{176}Lu/^{177}Hf CHUR = 0.0336. Depleted mantle values ^{176}Hf/^{177}Hf = 0.28325, ^{176}Lu/^{177}Hf = 0.0384 after Griffin et al. (2000). For zircon grains with ages <1,500 Ma, the ^{206}Pb/^{238}U age was used, while for zircon >1,500 Ma, the ^{207}Pb/^{206}Pb age was used Spencer et al. (2016). Further technical details regarding standards and reduction of results in included in the supplemental File SF1.

We have complemented our dataset with 18 Paleozoic and Mesozoic U–Pb detrital zircon samples from Okawa et al. (2013) (16 Samples newly coded OK) and Isozaki et al. (2014) (2 samples newly coded IS; Fig. 2; full site description in SF-1). In addition, we have extracted the zircon U–Pb from 8 plutons that intruded the fore-arc basin of SK (Plutons coded as OSO; Osozawa et al, 2019). Five out of these eight plutonic units also include Hf isotope analyses in zircons: one from Hikami granite and four from Aptian-Albian plutons (Tono, Hondera, Kesengawa and Hitokabe; Fig. 2; SF-1). We used the software package BAD-ZUPA (SF1-3) to quantitatively study the dominant zircon populations in the detrital zircon spectra, in addition to kernel density estimations and multi-dimensional scaling (Vermeesch, 2018). BAD-ZUPA is capable of automatically identifying the statistically significant peaks and valleys (at a 95% confidence), their most probable age, and the uncertainty of it.

Our sample from Hikami Granite (Kita13) displays no inherited zircons and a weighted average age of 435 ± 2.3 Ma (SF1). This age is compatible with previously published ages from U-Pb in zircons (OSO-08 in SF1, 442.4 ±9.8 Ma, and 449.2 ±4.5 Ma, Osozawa et al., 2019) and other methods (Ehiro et al., 2016 and references therein). Cretaceous granitoids samples from the Osozawa et al., (2019: OSO-01 to OSO-07) show ages between 120 and 110 Ma (see SF1).

In general terms, detrital zircon age spectra of samples from the Kitakami forearc present unimodal or bimodal age distributions whose main peak is increasingly young in tandem with the stratigraphy (Fig. 3). With the single exception of the Orikabetoge formation (Kita17, IS1) the maximum depositional ages, defined by the youngest concordant analysis, are in line with the biostratigraphic constraints (Fig. 3). Silurian and Devonian samples (Kita17, 12, 07; OK1-3 and IS1) have a unimodal distribution with a late Silurian to early Devonian maxima, similar to the ages from Hikami granite. Carboniferous samples Kita06 and OK4 are bimodal with the former late Silurian peak and a major Carboniferous one (~355 Ma) whereas IS2 show a wide unimodal distribution with a peak in 356 but including the Silurian-Devonian maxima in the distribution. All Permo-Triassic samples (Kita16, 11,02,05 and OK5-10) are unimodal with a Permian (290-260 Ma) peak except for OK10 (Late Triassic), which shows a minor Triassic peak. Jurassic and Cretaceous samples are unimodal (OK11, Kita04, 15), bimodal (OK12, 13, Kita10, 01), or multimodal (OK14 and 16). The Permian peak is represented in all the samples and an early Jurassic one (~180-190 Ma) is common to all but OK11 and Kita04. The youngest Cretaceous sample (OK16) shows a Cretaceous peak (~130 Ma). The Cenozoic samples present a prominent

Cretaceous peak (~105 Ma) with ages similar to the SKM Cretaceous granitoids and a smaller sub-recent peak (with zircon ages from Miocene to Quaternary). Precambrian zircons are statistically not relevant, 12 samples contained 0 Precambrian zircons, and the others just a few, which never cluster. These Precambrian zircons occur mostly in pre-Permian, Jurassic and Cretaceous samples. Age spectra and a composite spectrum with all samples (Figs. 3 and 4) show that younger populations contain very little to no zircon from the oldest representative peak. This is especially noticeable in Permian-Mesozoic samples, which have no or negligible amounts of pre-Permian zircons; and Cenozoic samples, whose spectra display no zircons older than ~120 Ma.

A composite age spectrum of all detrital samples define the synthetic dominant zircon populations for SKFB (Fig. 4). The number of pre-Cambrian zircons is residual (n = 190, 11%), none of the peaks is statistically relevant (Furukawa et al., submitted). If we consider only the total amount of Precambrian zircons, 3 peaks are significant: ~600 Ma, 1Ga and 1.9 Ga. We identified 6 synthetic dominant zircon populations at 430 ± 20, 360 ± 10, 270 ± 20, 184 ± 12, 112 ± 22, and 7 ± 7 Ma. We have plotted all individual samples in a multi-dimensional scaling (MDS) map (Vermeesch, 2013) against and the synthetic zircon population ages (Fig. 5; Spencer and Kirkland, 2016). MDS transforms a matrix of pairwise similarities (the D value from the Kolmogorov-Smirnov test) into a cartesian two-dimensional space showing all detrital zircon populations considered. On a MDS diagram distances represent the degree of similarity, the smaller the distance between two samples the more similar they are (Vermeesch 2013). The plot is dimensionless and values range between 0, and 1 on each axis. A distance of 0 between two samples means a perfect match and 1, no overlap between two distributions). The MDS map displays three clusters: the Pre-Permian samples; the Permo-Mesozoic samples and the Cenozoic samples.

The $^{176}Hf/^{177}Hf$ isotopic signature in zircons represents a proxy to estimate when the rock that crystalized such zircons was extracted from the mantle and to diagnose crustal reworking through time, where successive samples define a Hf evolution array (e.g. Spencer et al., 2019). Hf isotopic analyses of Hikami samples (Kita13 and OSO-08) have initial εHf values of -10 to +1 (Fig. 6A). The εHf values for the SKM

Cretaceous granitoids (OSO-01 to 07) ranges from 5 to 13, although other Tohoku areas (see Osozawa et al., 2019) exhibit a wider range (from -20 to 15), being from 0 to 15 the most concentrated area (Fig. 6A). Precambrian zircons show very variable εHf signatures, ranging from -20 to positive values close to the depleted mantle curve (Fig. 6B). No zircon older than 1.5 Ga has positive values. older than The Phanerozoic detrital zircon Hf evolution through the stratigraphy shows an εHf increase from ~430 Ma, with initial εHf values very similar to those of Hikami granite, to ~360 Ma where εHf values range from ~0 to ~10. From ~360 Ma, εHf trend increases with a less pronounced slope but losing all the less juvenile sources to ~270 Ma, where values get close to the depleted mantle curve. From there εHf decreases until ~112 Ma following a typical crustal residence trend. At around 112 Ma detrital zircon register, as in the igneous rocks values ranging from quite positive to about 0, mimicking the Cretaceous granitoids trend. The Hf array displays a similar effect in the sub recent population of zircons (Fig. 6B)

4. Discussion

The new (samples coded Kita) and reappraised (OK, IS and OSO samples from Okawa et al., 2013; Isozaki et al., 2014 and Osozawa et al., 2019, respectively) provide a crucial source of information to understand the Phanerozoic crustal history of Japan. The detrital zircon spectra through the stratigraphic column of SKFB revealed that most samples present unimodal or bimodal age peaks; younging upwards maximum depositional ages comparable to their biostratigraphic ages; and with minor to no Precambrian contribution (Figs. 3 and 6). A synthetic detrital zircon spectra considering all new and literature samples from SKM has 6 statistically significant populations at 430 ± 20, 360 ± 10, 270 ± 20, 184 ± 12, 112 ± 22, and 7 ± 7 Ma (Figs. 3, 4 and 5). All samples but Kita17 showed maximum depositional ages in line with the biostratigraphic age (Figs. 2 and 3). The youngest concordant zircons from Orikabetoge formation (Kita17 and IS1) are significatively younger than its published biostratigraphic age (~30 m.yrs). Its zircon distribution is, nonetheless, very similar to the other Silurian units. Both samples were collected in the same area and we cannot rule out that samples were collected in a Devonian unit since published literature mentions the lithological similarities between Silurian and Devonian clastic rocks in the area and geologic relationships are often obscured by minimal rock exposure (Ehiro et al., 2016).

4.1 Provenance of the South Kitakami Forearc

The sedimentary system of the Japanese forearc in SKM experienced limited sedimentary reworking of older forearc material and little sediment support from the cratonic and orogenic areas located to the west (present day coordinates). The major peaks in each sample (Fig. 3; Okawa et al., 2013; Isozaki et al., 2014) deviate very little from the dominant synthetic zircon age populations (430 ± 20, 360 ± 10, 270 ± 20, 184 ± 12, 112 ± 22, and 7 ± 7 Ma). Additionally, samples fall into three categories defined by the range of dominant zircon age populations (Fig. 4) pre-Permian, Permian-Mesozoic, and Cenozoic. The zircon support to the basin is controlled therefore by several detrital zircon forming events (coincident with the synthetic populations) and by two major time boundaries (late Carboniferous-early Permian and late Cretaceous) when the older arc and forearc stopped supporting zircons to the basin.

The paucity of Precambrian zircons (190/1991, ~10%) indicate that the volcanic arc has acted as a long term barrier impending transport of zircons from any craton. The combined Precambrian age spectra shows three main populations (Fig. 6B) at ~600, ~1000 and 1900 Ma, and two minor peaks at ~1500 and ~2800 Ma, which are consistent with a minor inflow of sediment to the forearc basin from South China Craton where the proto-Japan arc was likely located until the Triassic (Isozaki, 2019). So far, the 1900 Ma peak has not occured in NE Gondwana and the ~1000 Ma one is largely absent in North China (e.g. Zhao et al., 2017). The disappearance of Precambrian zircons during the Permian–Triassic times and reappearance in the SKM record from the Jurassic might be indicative of the Permo–Triassic collisional events in east-central China (e.g. Isozaki, 1997; Ernst et al., 2007) and its sedimentary dynamics, we cannot rule out minor contributions from North China from after such collision.

Despite the SKFB preserves an almost continuous stratigraphy from Silurian to Cretaceous, the prospective pre-Cretaceous arc-related sources of zircons to the basin are generally lacking. Apart from some tuffs intercalated in the pre-Permian stratigraphy (SF1), plutonic rocks older than Cretaceous are extremely scarce in SKM in particular and Japan in general (Fig. 1). In the SKM, the Silurian Hikami Granite (and equivalent plutons not cropping out) could represent the main source for the 430 ± 20 population. The only putative sources for the 360 ± 10 population are minor tuffs (Fig. 2; SF1). No sources for 270 ± 20 and 184 ± 12 Ma populations have been identified so far in SK, being the nearest in age and location the Carboniferous-Permian Wariyama granite in the Abukuma Mountains, to the south (~300 Ma., Tsutsumi et al., 2010; Tsuchiya et al., 2014). The Permian zircon population is the most prominent not only in SK but also in other in other Permo-Mesozoic forearc basins and accretionary complexes in SW Japan (e.g. Isozaki et al., 2010; Zhang et al., 2019). However, Permian igneous rocks are almost absent in the Japanese record excepting the Hida Belt. In contrast, Miocene to recent andesites and rhyolitic flows and, especially, Cretaceous large batholiths abound in all the Japanese archipelago (Figs. 1 and 2).

4.2 Hf isotopes: Japan sinks, Japan melts

The Precambrian population of zircons in Kita samples is too scarce (n = 49) to interpret important trends in the crustal residence of the source areas. Nonetheless, we think it is a useful preliminary constraint into the contested proto-Japan paleogeography (South China vs. North China, e.g. Isozaki, 2019; Wakita et al., 2021). We distinguished two groups in the Kita samples Hf array (Fig. 6B). Zircons of the ~1.9 Ga population and all the older show variable negative values of εHf. The younger populations (~1 Ga and ~600 Ma) have very mixed values, from very positive to negative, suggesting a mixing between significant amounts of newly extracted from the mantle material and other crustal sources. Our Precambrian results are compatible with a provenance from Cathaysia and/or Yangtze blocks (South China craton, Fig. 1), with similar detrital zircon populations and εHf array (Cawood et al., 2018; Wan et al., 2019). In contrast, North China's 1.9 Ga population has quite positive εHf values (Xia et al., 2008). Further data is necessary to confirm such provenance, but with the present dataset, we are inclined towards a proto-Japan arc being part of a Greater South China continent (Isozaki et al., 2014; 2015).

The evolution of Hf in the Phanerozoic zircons through the stratigraphy (Fig. 6) shows a Hf array that starts with similar values to the Hikami granite (Kita 13 and OSO 08 from Osozawa et al., 2019). The age similarity and Hf signature suggest that Hikami and/or very similar non-preserved Silurian plutons fed the forearc basin during the Silurian-Carboniferous times. The εHf/Ma trend displays progressively more juvenile (positive) values as the zircon population gets younger. This indicates that the sources of Devonian and Early Carboniferous zircons mixed depleted mantle material with the previous SKM crust. From ~360 Ma, the trajectory keeps on increasing until ~270 Ma with very positive values in the proximity of the depleted mantle curve. Remarkably, the trend from 360 to 270 Ma loses most of the less juvenile contribution, indicating little crustal mixing of the sources of Carboniferous and Permian zircons. We interpret that the steep εHf/Ma trajectory from 450 to 270 Ma implies a progressively loss of the original proto-Japan crust. At the beginning of such a process (from ~450 to ~360) the growing contribution in the SK crust from the depleted mantle was mixing with the previous crust. From ~360 to ~270 Ma less and less crustal mixing occur, indicating an almost complete loss of the previous crust during the Late Paleozoic. This process ended with a complete crustal replacement in the Permian.

From ~270 Ma, εHf trend decreases until ~112 Ma following a typical crustal residence trend. We interpret the trend as a period in which the Permian new crust matured and where, despite the Jurassic minor flare up, new mantle input was minor. At around 112 Ma detrital zircon register, analog to the igneous rocks, values ranging from quite positive to about 0, the same as in the sub recent population of zircons (Fig. 6B). It indicates a lot of mixing between the Permian crust and new inputs from the depleted mantle. Considering that the majority of the present-day Japan arc crust is a Cretaceous large batholith, we support that the majority of the Japanese crust melted during a punctual and diachronic event (in Tohoku ~112 Ma, progressively younger to the South and west, Osozawa et al., 2019). Some authors attributed the magmatic event to the subduction of the Izanagi plate's ridge below Japan (e.g. Maruyama and Seno, 1986; Maruyama et al., 1997), although the kinematics, timing and orientation of the ridge subduction are disputed (see Wu and Wu, 2020 for discussion and references).

The gap in the SKFB zircon record from the Cretaceous population to the subrecent one hinders the crustal evolution during the Late Cretaceous and Paleogene. Other fragments of the fore-arc basin like the Izumi Group in SW Japan) may shed light about the crustal evolution since samples general show unimodal detrital zircon peak at ~80 Ma, however Hf signatures have not been studied so far (Aoki et al., 2012). The sub-recent population shows a range of juvenile εHf (from ~0 to ~12). This indicates, again, mixing of new depleted mantle sources and former crust. In this case, we think that the retreat of the arc after the Miocene opening of the Japan Sea (van Horne et al., 2017 and references therein) explains best the Miocene to recent Hf trend.

4.3 Flaring up and dragging Japan down

The Phanerozoic zircon pool of individual sample spectra shows dominant populations that are roughly coeval and little Precambrian zircon sources (Fig. 3). The dominant populations, confirmed by the composite Phanerozoic detrital zircon spectra of SKFB (1801 out of 1991 zircons), are late Silurian, early Carboniferous, Permian, early Jurassic, Aptian-Albian and sub-recent in age. The youngest population in each spectrum does not get progressively younger as we go upwards in the stratigraphy (Fig. 3), or not to a significant level. For example, OK6 (Permian strata) has a younger peak than all Triassic samples whose youngest peak is Permian but one. Older populations get progressively less important, to finally disappear forever (Fig. 3). In addition to the progressively loss of previous sources, both the individual and the composite spectra evince that Post-Carboniferous samples do not display any pre-Permian zircon age peaks (Figs. 3 and 4). Likewise, Cenozoic samples do not show any pre-Cretaceous zircon age peaks (Figs. 3 and 4). This leaves three groups (Pre-Permian, Permian-Mesozoic and Cenozoic, Fig. 4) that are further justified by the use of MDS by comparing the SKFB samples with synthetic age populations (Fig. 5). In the MDS map, the Pre-Permian samples cluster near the early Silurian population with a trend as samples go upwards in the column towards the early Carboniferous. Following a similar pattern, the

Permian-Cretaceous samples cluster near the ~270 ± 20 Ma synthetic population with a trend towards the Jurassic maxima (184 ± 12 Ma). Finally, the Cenozoic samples cluster near the ~112 ± 22 Ma but not far from the 7 ± 7 Ma population. The Hf array indicates that the process responsible for the two main events where previous sources disappear could not be the same.

SKFB contains an almost continuous forearc stratigraphy from late Silurian to early Cretaceous (Fig. 2), and most of other geological evidence in the archipelago points to an uninterrupted subduction below Japan during, at least, 400 m.yr (e.g. Maruyama et al., 1997; Isozaki et al., 2010). If arc activity had been continuous and approximately at a constant rate, we would have found a progressively younger maximum depositional age pointing to a progressively younger arc source feeding the basin. However, we found an age consistency of the dominant populations through the stratigraphy, suggesting that significant zircon forming events in the arc were followed by relatively still periods with lesser magmatism. We propose that the main populations represent magmatic flare-ups. Some of these hypothesized flare-ups but the most recent seem to occur coeval to main HP-LT metamorphic events (Fig. 1): (1) Silurian – Fuko Pass; (2) early Carboniferous – Renge; and (3) the most obvious, Cretaceous – Sanbagawa, where Cretaceous batholiths paired with coeval HP-LT and/or, in the case of the sub-recent populations with the opening of the Japan Sea (Fig. 1). The cyclic HP-LT metamorphic together with coeval LP-HT metamorphism and anatexis (Miyashiro's 'paired metamorphic belt' concept (1961)) are common in long-lived Pacific type orogeny (e.g., western USA: Snow and Barns, 2006). The only tectonic events close to coeval to the Permian maxima is the collision of Maizuru arc and the sub-recent population fits in time with the opening of the Japan Sea. We could not find any event that can explain the Jurassic zircon maxima.

The progressive depletion of older populations upwards in the stratigraphy indicates the loss of the igneous source and little reworking of previous strata. Low rates of basin reworking suggest a protracted subsidence keeping the basin away from erosion. The fading of the older zircon sources may be related to its burial below newer arc material; high erosion rates enough to completely erode the source rocks; or tectonic erosion removing the oldest section of the arc from below. Complete burial would require a continuous arc production. Our zircon record evidences intermittent magmatic flare-ups instead. Large amounts of magmatism during a flare-up could be blamed for the burial of older sources. In such case, it would be expected that these older sources became more present after several million years of erosion of the flare-up, but we found the opposite. The complete erosion of previous arcs manifest similar setbacks: if the arc had been repeatedly dismantled due to high erosion rates, we would have found Precambrian zircons coming from the cratons each time the arc did not represent a sedimentary barrier. Previous studies (e.g. Suzuki et al., 2010; Isozaki et al., 2010) suggested that he Japan arc has undergone frequent periods of tectonic erosion since the Silurian, removing significant parts of its geological record. Tectonic erosion (von Huene and Lallemand, 1990) can explain both the disappearance of older arc sources, the mixing of Hf signatures becoming progressively more juvenile, and continuous subsidence of the forearc.

Nonetheless, the main two events when the older sources completely disappeared (Late Carboniferous - Early Permian and Cretaceous) are hardly explained by tectonic erosion. During the late Carboniferous event, the Hf array shows the arc crust was completely renewed (Fig. 6B). Delamination of the lithospheric mantle s.l. (e.g. Magni and Király, 2020) can explain the partial removal of the lower crust and the generation of mantle derived magmatism, whereas the consequent uplift produces a quick and intense denudation. We think this is the most plausible mechanism explaining the quick removal of the Precambrian crust in NE Japan and the subsequent Permian flare-up (Figs. 3 and 6B). Candidates triggering delamination in the overriding plate are a rapid arc retreat, for example due to slab roll-back, or collision of an arc or oceanic plateau that stagnated below Japan, resulting in an over-thickened crust and forming a convective drip at the base of the thickened lithosphere. So far, we have not been able to find compelling evidence of late Carboniferous widespread extension and development of large back-arc in the Japanese and East Asia margin (e.g. Shen et al., 2018). In contrast, the only collisional candidate (Maizuru; Fig 1) is too young and it is uncertain whether the magnitude of the collision was enough to precipitate a delamination event (Fig. 1, Kimura et al., 2019). The Hf signature of the Cretaceous zircon sources loss event suggests, in contrast to the late Carboniferous, a general mixing between the older and the juvenile crust. The crustal reworking time is coeval to the emplacement of the Cretaceous batholiths with frequent adakitic composition (Tsuchiya et al., 2014; Osozawa et al., 2019) that represents the bulk of today Japanese crust, and the final subduction of the Izanagi plate (c.f. Wu and Wu, 2020). We found appealing a cause effect relationship between the final subduction of the Izanagi ridge, the formation of slab windows and the development of a flare-up that adds new material from the depleted mantle and was capable of melting the majority of the Permian crust of Japan. We also think that the Miocene opening of the Japan Sea explains well the character of the sub-recent zircon population. The detrital zircons of SKFB tell us the hidden history of the missing record of Japan, a violent tale of flare-ups, crustal melting and lithospheric foundering.

5. Conclusions

The composite Phanerozoic detrital zircon spectra of the SKFB of Japan define dominant zircon age populations at ~430, ~360, ~270, ~180, ~112 and ~7 Ma. We found very few Precambrian zircons, which indicate the arc acted as a barrier for craton support during all Phanerozoic. In addition to these dominant populations, we recognize a progressive disappearance of older sources and three time intervals with very few to no zircons: ~320 to 300 Ma; ~160 to 140 Ma and ~60 to 20 Ma. These gaps are coincident with tectonically still periods in the Japanese geology. The $^{176}Hf/^{177}Hf$ isotopic signature of the zircon spectra shows an εHf increase from ~430 Ma to ~270 Ma, when the Japanese crust became completely juvenile. From there εHf decreases until ~112 Ma following a typical crustal residence trend. At around 112 Ma detrital a quick event mixed the Permian crust with new input from the mantle. We found a similar effect in the sub recent population of zircons.

The SKFB detrital zircon record evinces a geological history punctuated by magmatic flare-ups, which produced large amounts of zircons; and periods with very little arc activity. The progressive disappearance of older sources of zircons reveals a protracted ~500 m.yr. of tectonic erosion, which hindered the crustal growth in Japan arc. Finally, Hf isotopes revealed two catastrophic events: A late Carboniferous loss of the Japanese crust, which we interpret as a delamination process and a Cretaceous melting of the entire arc, probably related with the subduction of the mid-oceanic ridge separating the Izanagi and Pacific plates.

Acknowledgements

We would like to thank Xiaofang He, Brad McDonald, and Noreen Evans for lab assistance. Hiroyuki Okawa and Soichi Osozawa kindly provided their datasets to be included in this paper. Research in the GeoHistory laser ablation Facility, John de Laeter Centre, Curtin University of Technology is supported by AuScope (auscope.org.au) and the Australian Government via the National Collaborative Research Infrastructure Strategy (NCRIS). The NPII multi-collector was obtained via funding from the Australian Research Council LIEF program (LE150100013). The constructive comments by Yukio Isozaki and an anonymous reviewer greatly improved the paper. This paper was funded by MEXT/JSPS KAKENHI Grant (15H05212, JP16F16329, 18H01299) and an "Ensemble Grant for Young Researchers"(Tohoku University). DPG also thanks a lifetime of company provided by Christopher John Cornell. You broke your rusty cage, now the cold Earth is your bed.

Figure captions

Figure 1: A) Location of the main continental blocks and cratons of East Asia (modified after Harada et al., 2021). B) Simplified geological map of Japan based on the Seamless digital geological map of Japan 1: 200,000 (2021). C) Simplified chronology of the main tectonic events recorded in the Japanese active margin.

Figure 2: South Kitakami synthetic geological map and stratigraphy showing the sampling locations based on the Seamless digital geological map of Japan 1: 200,000 (2021). Samples coded Kita are newly analyzed, OK after Okawa et al. (2013), IS after Isozaki et al. (2014) and samples coded OSO after Osozawa et al. (2019).

Figure 3: Zircon spectra in the Kita (new dataset), OK (Okawa et al., 2013) and IS (Isozaki et al., 2014) samples from the South Kitakami forearc basin.

Figure 4: A) Composite spectra of all detrital samples. B) Composite spectra of all pre-Permian samples. C) Composite spectra of the Permian-Mesozoic samples. D) Spectra of the three Cenozoic samples studied.

Figure 5: Multidimensional Scaling map of all detrital zircon samples depicting the similarities and evolution of the three identified groups based on the total loss of the previous distributions (pre-Permian, Permian-Mesozoic and Cenozoic)

Figure 6: A) εHf in zircon respect to their U-Pb zircon age for the Hikami Granite (Silurian) and the Cretaceous granitoids of South Kitakami and surroundings (from Osozawa et al., 2019) B) εHf in the detrital zircons vs. their ages (Kita samples).

Supplemental files

SF1: In detail sample description and sampling location including pictures of the sampled rocks.

SF2: KML Google Earth file with the sampling location

SF3: Table with U-Pb and Hf results

References

1. Aoki, K., Isozaki, Y., Yamamoto, S., Maki, K., Yokoyama, T. and Hirata, T., 2012. Tectonic erosion in a Pacific-type orogen: Detrital zircon response to Cretaceous tectonics in Japan. Geology 40, 1087-1090. https://doi.org/10.1130/G33414.1

2. Bouvier, A., Vervoort, J.D., Patchett, P.J., 2008. The Lu-Hf and Sm-Nd isotopic composition of CHUR: Constraints from unequilibrated chondrites and implications for the bulk composition

of terrestrial planets. Earth and Planetary Science Letters 273, 48–57. https://doi.org/10.1016/j.epsl.2008.06.010

3. Cawood, P.A., Zhao, G., Yao, J., Wang, W., Xu, Y., Wang, Y., 2018. Reconstructing South China in Phanerozoic and Precambrian supercontinents. Earth-Science Reviews 186, 173–194. https://doi.org/10.1016/j.earscirev.2017.06.001

4. Ehiro, M., Tsujimori, T., Tsukada, K., Nuramkhaan, M., 2016. Palaeozoic basement and associated cover., in Moreno T. et al., eds, The Geology of Japan: Bath, Geological Society Publishing House, p. 25–60. https://doi.org/10.1144/goj.2

5. Ernst, W.G., Tsujimori, T., Zhang, R. and Liou, J.G., 2007. Permo-Triassic collision, subduction-zone metamorphism, and tectonic exhumation along the East Asian continental margin. Annual Review of Earth and Planetary Sciences 35, 73-110. https://doi.org/10.1146/annurev.earth.35.031306.140146

6. Geological Survey of Japan, AIST (ed.). 2021. Seamless digital geological map of Japan 1: 200,000 V2. January 22, 2021 version. Geological Survey of Japan, AIST, https://gbank.gsj.jp/seamless/index_en.html

7. Griffin, W.L., Pearson, N.J., Belousova, E., Jackson, S.E., van Achterbergh, E., O'Reilly, S.Y., Shee, S.R., 2000. The Hf isotope composition of cratonic mantle: LAM-MC-ICPMS analysis of zircon megacrysts in kimberlites. Geochimica et Cosmochimica Acta 64, 133–147. https://doi.org/10.1016/S0016-7037(99)00343-9

8. Harada, H., Tsujimori, T., Kunugiza, K., Yamashita, K., Takayanagi, H., Iryu, Y., 2021. The $\delta^{13}C$-$\delta^{18}O$ variations in marble in the Hida Belt, Japan. Island Arc 30, e12389. https://doi.org/10.1111/iar.12389

9. Ishiwatari, A., Tsujimori, T., 2003. Paleozoic ophiolites and blueschists in Japan and Russian Primorye in the tectonic framework of East Asia: A synthesis. Island Arc 12, 190–206. https://doi.org/10.1046/j.1440-1738.2003.00390.x

10. Isozaki, Y., 2019. A visage of early Paleozoic Japan: Geotectonic and paleobiogeographical significance of Greater South China. Island Arc, 28, e12296. https://doi.org/10.1111/iar.12296

11. Isozaki, Y., 1997. Contrasting two types of orogen in Permo-Triassic Japan: accretionary vs. collisional. Island Arc 6, 2–24. https://doi.org/10.1111/j.1440-1738.1997.tb00038.x

12. Isozaki, Y., Aoki, K., Nakama, T., Yanai, S., 2010. New insight into a subduction-related orogen: A reappraisal of the geotectonic framework and evolution of the Japanese Islands. Gondwana Research, 18, 82-105. https://doi.org/10.1016/j.gr.2010.02.015

13. Isozaki, Y., Aoki, K., Sakata, S. and Hirata, T., 2014. The eastern extension of Paleozoic South China in NE Japan evidenced by detrital zircon. GFF 136, 116–119. https://doi.org/10.1080/11035897.2014.893254

14. Isozaki, Y., Ehiro, M., Nakahata, H., Aoki, K., Sakata, S., Hirata, T., 2015. Cambrian plutonism in Northeast Japan and its significance for the earliest arc-trench system of proto-Japan: New U-Pb zircon ages of the oldest granitoids in the Kitakami and Ou Mountains. Journal of Asian Earth Sciences 108, 136–149. https://doi.org/10.1016/j.jseaes.2015.04.024

15. Ito, T., Kojima, Y., Kodaira, S., Sato, H., Kaneda, Y., Iwasaki, T., Kurashimo, E., Tsumura, N., Fujiwara, A., Miyauchi, T., Hirata, N., Harder, S., Miller, K., Murata, A., Yamakita, S., Onishi, M., Abe, S., Sato, T., Ikawa, T., 2009. Crustal structure of southwest Japan, revealed by the integrated seismic experiment Southwest Japan 2002. Tectonophysics 472, 124–134. https://doi.org/10.1016/j.tecto.2008.05.013

16. Jahn, B.M., 2004. The Central Asian Orogenic Belt and growth of the continental crust in the Phanerozoic. Geological Society, London, Special Publications 226, 73–100. https://doi.org/10.1144/GSL.SP.2004.226.01.05

17. Magni, V., Király, Á., 2020. Delamination, in: Reference Module in Earth Systems and Environmental Sciences. Elsevier. https://doi.org/10.1016/B978-0-12-409548-9.09515-4

18. Maruyama, S. and Seno, T., 1986. Orogeny and relative plate motions: example of the Japanese Islands. Tectonophysics 127, 305-329. https://doi.org/10.1016/0040-1951(86)90067-3

19. Maruyama, S., Isozaki, Y., Kimura, G. and Terabayashi, M., 1997. Paleogeographic maps of the Japanese Islands: Plate tectonic synthesis from 750 Ma to the present. Island Arc 6, 121-142.

20. Miyashiro, A. 1961. Evolution of metamorphic belts. Journal of Petrology 2, 277–311.

21. Morel, M.L.A., Nebel, O., Nebel-Jacobsen, Y.J., Miller, J., Vroon, P.Z., 2008. Hafnium isotope characterization of the GJ-1 zircon standard by solution and laser ablation MC-ICPMS. Chemical Geology. Chemical Geology 225, 231–235. https://doi.org/10.1016/j.chemgeo.2008.06.040

22. Okawa, H., Shimojo, M., Orihashi, Y., Yamamoto, K., Hirata, T., Sano, S.I., Ishizaki, Y., Kouchi, Y., Yanai, S. and Otoh, S., 2013. Detrital zircon geochronology of the Silurian–Lower Cretaceous continuous succession of the South Kitakami belt, northeast Japan. Memoir of the Fukui Prefectural Dinosaur Museum 12, 35-78. https://dl.ndl.go.jp/info:ndljp/pid/10970636

23. Osozawa, S., Usuki, T., Usuki, M., Wakabayashi, J., Jahn, B., 2019. Trace elemental and Sr-Nd-Hf isotopic compositions, and U-Pb ages for the Kitakami adakitic plutons: Insights into interactions with the early Cretaceous TRT triple junction offshore Japan. Journal of Asian Earth Sciences 184, 103968. https://doi.org/10.1016/j.jseaes.2019.103968

24. Otoh, S., Yamakita, S. and Yanai, S., 1990. Origin of the Chichibu Sea, Japan: Middle Paleozoic to Early Mesozoic plate construction in the northern margin of the Gondwana Continent. *Tectonics*, *9*(3), pp.423-440.

25. Ozawa, K., Maekawa, H., Shibata, K., Asahara, Y., Yoshikawa, M., 2015. Evolution processes of Ordovician–Devonian arc system in the South-Kitakami Massif and its relevance to the Ordovician ophiolite pulse. Island Arc 24, 73–118. https://doi.org/10.1111/iar.12100

26. Pastor-Galán, D., Nance, R.D., Murphy, J.B., Spencer, C.J., 2019. Supercontinents: myths, mysteries, and milestones. Geological Society, London, Special Publications 470, 39–64. https://doi.org/10.1144/SP470.16

27. Sasaki, M., 2003. Early Cretaceous sinistral shearing and associated folding in the South Kitakami Belt, northeast Japan. Island Arc 12, 92–109. https://doi.org/10.1046/j.1440-1738.2003.00383.x

28. Scherer, E., Münker, C., Mezger, K., 2001. Calibration of the Lutetium-Hafnium Clock. Science 293, 683–687. https://doi.org/10.1126/science.1061372

29. Shen, L., Yu, J.H., O'Reilly, S.Y. and Griffin, W.L., 2018. Tectonic switching of southeast China in the Late Paleozoic. *Journal of Geophysical Research: Solid Earth*, *123*(10), pp.8508-8526.

30. Shimojo, M., Otoh, S., Yanai, S., Hirata, T., Maruyama, S., 2010. LA-ICP-MS U-Pb Age of Some Older Rocks of the South Kitakami Belt, Northeast Japan. Journal of Geography 119, 257–269 (in Japanese with an English abstract). https://doi.org/10.5026/jgeography.119.257

31. Snow, A.W. and Barns, C.G. (2006) Geological Studies in the Klamath Mountains Province, California and Oregon: A volume in honor of William P. Irwin. GSA Special Paper 410, 505 p. https://doi.org/10.1130/SPE410

32. Spencer, C.J., Kirkland, C.L., Prave, A.R., Strachan, R.A., Pease, V., 2019. Crustal reworking and orogenic styles inferred from zircon Hf isotopes: Proterozoic examples from the North Atlantic region. Geoscience Frontiers, Climate change impacts on environmental geosciences 10, 417–424. https://doi.org/10.1016/j.gsf.2018.09.008

33. Spencer, C.J., Kirkland, C.L., Taylor, R.J.M., 2016. Strategies towards statistically robust interpretations of in situ U–Pb zircon geochronology. Geoscience Frontiers 7, 581–589. https://doi.org/10.1016/j.gsf.2015.11.006

34. Spencer, C.J. and Kirkland, C.L., 2016. Visualizing the sedimentary response through the orogenic cycle: A multidimensional scaling approach. *Lithosphere*, *8*(1), pp.29-37.

35. Spencer, C.J., Roberts, N.M.W., Santosh, M., 2017. Growth, destruction, and preservation of Earth's continental crust. Earth-Science Reviews 172, 87–106. https://doi.org/10.1016/j.earscirev.2017.07.013

36. Stern, C.R., 2011. Subduction erosion: Rates, mechanisms, and its role in arc magmatism and the evolution of the continental crust and mantle. Gondwana Research 20, 284–308. https://doi.org/10.1016/j.gr.2011.03.006

37. Suzuki, K., Maruyama, S., Yamamoto, S., Omori, S., 2010. Have the Japanese Islands Grown?: Five"Japan"s Were Born, and Four"Japan"s Subducted into the Mantle. Journal of Geography 119, 1173–1196 (in Japanese with an English abstract). https://doi.org/10.5026/jgeography.119.1173

38. Tagiri, M., Dunkley, D.J., Adachi, T., Hiroi, Y., Fanning, C.M., 2011. SHRIMP dating of magmatism in the Hitachi metamorphic terrane, Abukuma Belt, Japan: Evidence for a Cambrian volcanic arc. Island Arc 20, 259–279. https://doi.org/10.1111/j.1440-1738.2011.00764.x

39. Tsuchiya, N., Takeda, T., Tani, K., Adachi, T., Nakano, N., Osanai, Y. and Kimura, J.I., 2014. Zircon U–Pb age and its geological significance of late Carboniferous and Early Cretaceous adakitic granites from eastern margin of the Abukuma Mountains, Japan. Journal of Geological Society of Japan 120, 37–51. https://doi.org/10.5575/geosoc.2014.0003

40. Tsutsumi, Y., Ohtomo, Y., Horie, K., Nakamura, K.I. and Yokoyama, K., 2010. Granitoids with 300 Ma in the Joban coastal region, east of Abukuma Plateau, northeast Japan. Journal of Mineralogical and Petrological Science 105, 320–327. https://doi.org/10.2465/jmps.091204

41. Tsujimori, T. and Itaya, T., 1999. Blueschist-facies metamorphism during Paleozoic orogeny in southwestern Japan: Phengite K–Ar ages of blueschist-facies tectonic blocks in a serpentinite melange beneath early Paleozoic Oeyama ophiolite. *Island Arc*, *8*(2), pp.190-205.

42. Tsujimori, T., 2017. Early Paleozoic jadeitites in Japan: An overview. Journal of Mineralogical and Petrological Sciences 112, 217–226. https://doi.org/10.2465/jmps.170406a

43. Van Horne, A., Sato, H., Ishiyama, T., 2017. Evolution of the Sea of Japan back-arc and some unsolved issues. Tectonophysics 710–711, 6–20. https://doi.org/10.1016/j.tecto.2016.08.020

44. Vermeesch, P., 2018. IsoplotR: A free and open toolbox for geochronology. Geoscience Frontiers 9, 1479–1493. https://doi.org/10.1016/j.gsf.2018.04.001

45. Vermeesch, P., 2013. Multi-sample comparison of detrital age distributions. Chemical Geology 341, 140–146. https://doi.org/10.1016/j.chemgeo.2013.01.010

46. von Huene, R. and Lallemand, S., 1990. Tectonic erosion along the Japan and Peru convergent margins. Geological Society of America Bulletin, 102, 704–720. https://doi.org/10.1130/0016-7606(1990)102<0704:TEATJA>2.3.CO;2

47. Wakita, K., Nakagawa, T., Sakata, M., Tanaka, N. and Oyama, N., 2021. Phanerozoic accretionary history of Japan and the western Pacific margin. *Geological Magazine*, *158*(1), pp.13-29.

48. Wan, Y., Xie, H., Dong, C., Kröner, A., Wilde, S.A., Bai, W., Liu, S., Xie, S., Ma, M., Li, Y., Liu, D., 2019. Chapter 14 - Hadean to Paleoarchean Rocks and Zircons in China, in: Van Kranendonk, M.J., Bennett, V.C., Hoffmann, J.E. (Eds.), Earth's Oldest Rocks (Second Edition). Elsevier, pp. 293–327. https://doi.org/10.1016/B978-0-444-63901-1.00014-9

49. Wu TJ., Wu, J., 2019. Izanagi-Pacific ridge subduction revealed by a 56 to 46 Ma magmatic gap along the northeast Asian margin. Geology. https://doi.org/10.1130/G46778.1

50. Xia, X., Sun, M., Zhao, G., Wu, F., Xu, P., Zhang, J., He, Y., 2008. Paleoproterozoic crustal growth in the Western Block of the North China Craton: Evidence from detrital zircon Hf and whole rock Sr-nd isotopic compositions of the Khondalites from the Jining Complex. Am J Sci 308, 304–327. https://doi.org/10.2475/03.2008.05

51. Zhang, X., Takeuchi, M., Lee, H.-Y., 2019. Tracing the origin of Southwest Japan using the Hf isotopic composition of detrital zircons from the Akiyoshi Belt. Terra Nova 31, 11–17. https://doi.org/10.1111/ter.12363

52. Zhao, T., Feng, Q., Metcalfe, I., Milan, L.A., Liu, G., Zhang, Z., 2017. Detrital zircon U-Pb-Hf isotopes and provenance of Late Neoproterozoic and Early Paleozoic sediments of the Simao and Baoshan blocks, SW China: Implications for Proto-Tethys and Paleo-Tethys evolution and Gondwana reconstruction. Gondwana Research 51, 193–208. https://doi.org/10.1016/j.gr.2017.07.012

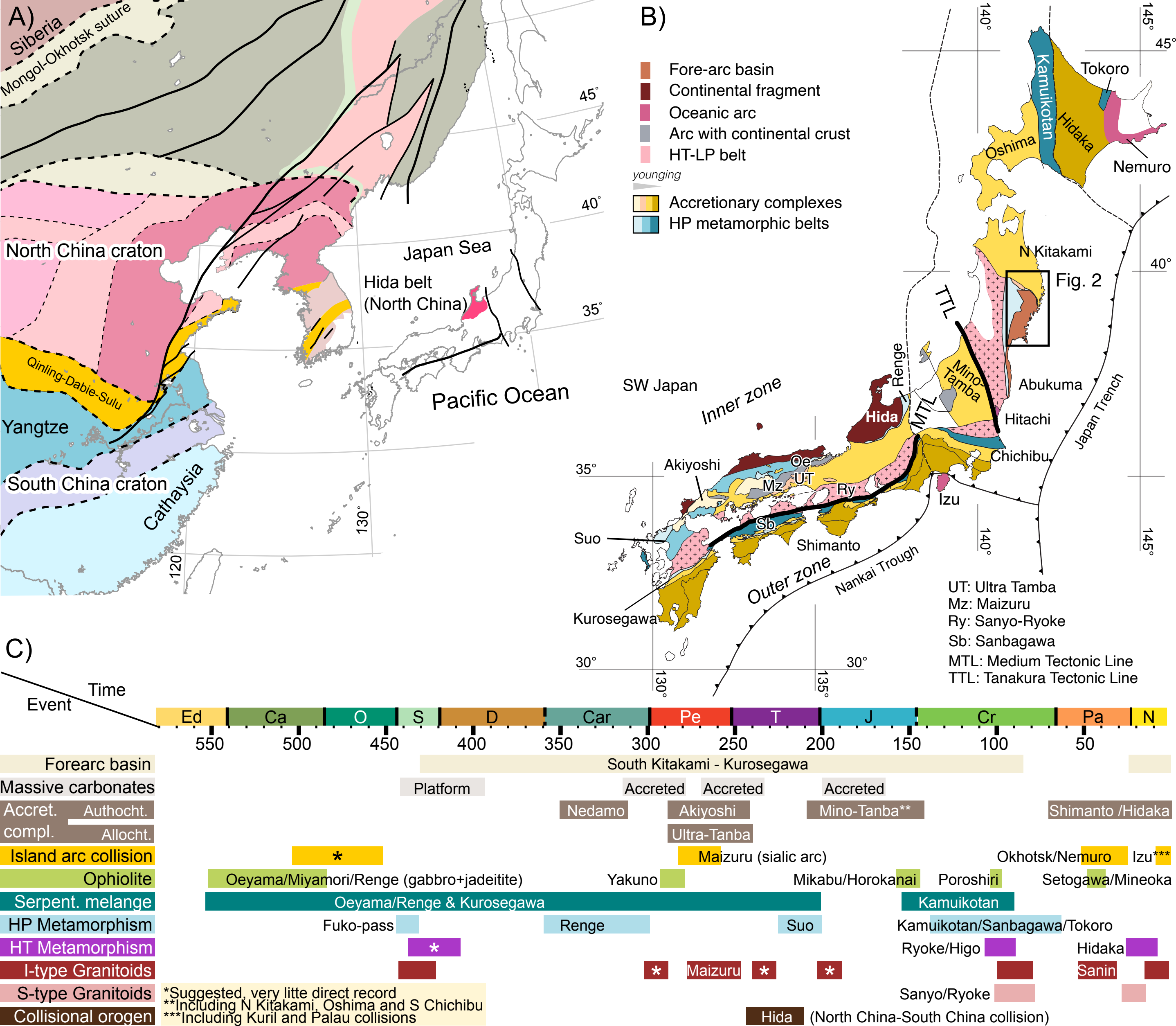

A)
Siberia
Mongol-Okhotsk suture
North China craton
Qinling-Dabie-Sulu
Yangtze
South China craton
Cathaysia
Japan Sea
Hida belt
(North China)
Pacific Ocean
B)
Fore-arc basin
Continental fragment
Oceanic arc
Arc with continental crust
HT-LP belt
younging
Accretionary complexes
HP metamorphic belts
Kamuikotan
Tokoro
Oshima
Hidaka
Nemuro
N Kitakami
Fig. 2
TTL
Renge
Mino-Tamba
Abukuma
Hitachi
Hida
MTL
Chichibu
SW Japan
Inner zone
Akiyoshi
Oe
UT
Mz
Ry
Izu
Suo
Sb
Shimanto
Outer zone
Nankai Trough
Japan Trench
Kurosegawa
UT: Ultra Tamba
Mz: Maizuru
Ry: Sanyo-Ryoke
Sb: Sanbagawa
MTL: Medium Tectonic Line
TTL: Tanakura Tectonic Line
C)
Time
Event
Ed
Ca
O
S
D
Car
Pe
T
J
Cr
Pa
N
550
500
450
400
350
300
250
200
150
100
50
Forearc basin
South Kitakami - Kurosegawa
Massive carbonates
Platform
Accreted
Accreted
Accreted
Accret. compl.
Authocht.
Allocht.
Nedamo
Akiyoshi
Mino-Tanba**
Shimanto /Hidaka
Ultra-Tanba
Island arc collision
*
Maizuru (sialic arc)
Okhotsk/Nemuro
Izu***
Ophiolite
Oeyama/Miyamori/Renge (gabbro+jadeitite)
Yakuno
Mikabu/Horokanai
Poroshiri
Setogawa/Mineoka
Serpent. melange
Oeyama/Renge & Kurosegawa
Kamuikotan
HP Metamorphism
Fuko-pass
Renge
Suo
Kamuikotan/Sanbagawa/Tokoro
HT Metamorphism
*
Ryoke/Higo
Hidaka
I-type Granitoids
*
Maizuru
*
*
Sanin
S-type Granitoids
Sanyo/Ryoke
Collisional orogen
Hida
(North China-South China collision)
*Suggested, very litte direct record
**Including N Kitakami, Oshima and S Chichibu
***Including Kuril and Palau collisions

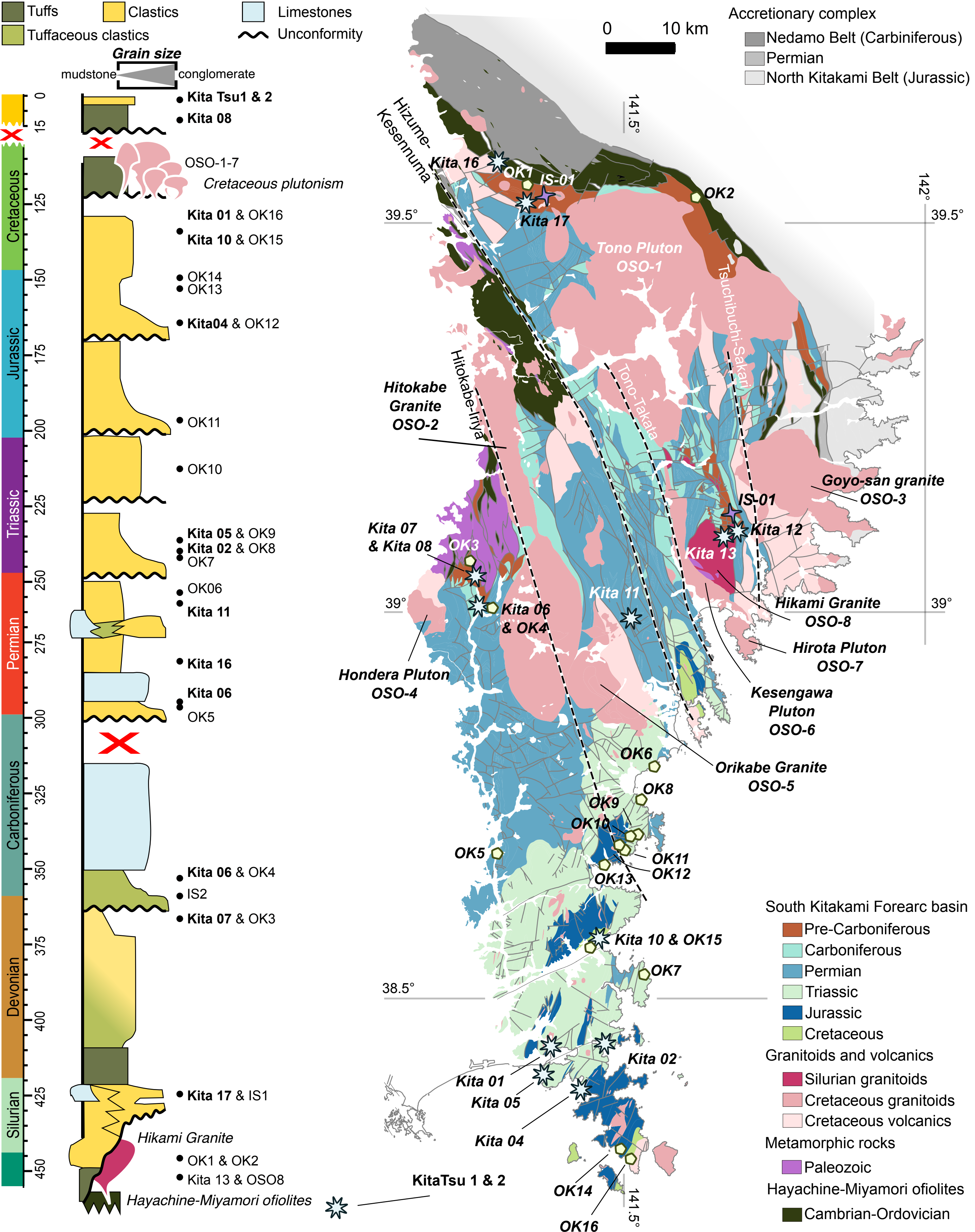

Tuffs
Clastics
Limestones
Tuffaceous clastics
Unconformity
Grain size
mudstone
conglomerate
Cretaceous
Jurassic
Triassic
Permian
Carboniferous
Devonian
Silurian
Kita Tsu1 & 2
Kita 08
OSO-1-7
Cretaceous plutonism
Kita 01 & OK16
Kita 10 & OK15
OK14
OK13
Kita04 & OK12
OK11
OK10
Kita 05 & OK9
Kita 02 & OK8
OK7
OK06
Kita 11
Kita 16
Kita 06
OK5
Kita 06 & OK4
IS2
Kita 07 & OK3
Kita 17 & IS1
Hikami Granite
OK1 & OK2
Kita 13 & OSO8
Hayachine-Miyamori ofiolites
KitaTsu 1 & 2
0
10 km
Accretionary complex
Nedamo Belt (Carbiniferous)
Permian
North Kitakami Belt (Jurassic)
Hizume-Kesennuma
Hitokabe-Iriya
Tono-Takata
Tsuchibuchi-Sakari
Tono Pluton
OSO-1
Hitokabe Granite
OSO-2
Goyo-san granite
OSO-3
Hondera Pluton
OSO-4
Orikabe Granite
OSO-5
Kesengawa Pluton
OSO-6
Hirota Pluton
OSO-7
Hikami Granite
OSO-8
Kita 07 & Kita 08
Kita 06 & OK4
Kita 12
Kita 13
IS-01
Kita 17
OK1
OK2
OK3
OK5
OK6
OK7
OK8
OK9
OK10
OK11
OK12
OK13
OK14
OK16
Kita 10 & OK15
Kita 01
Kita 05
Kita 04
Kita 02
39.5°
39°
38.5°
141.5°
142°
South Kitakami Forearc basin
Pre-Carboniferous
Carboniferous
Permian
Triassic
Jurassic
Cretaceous
Granitoids and volcanics
Silurian granitoids
Cretaceous granitoids
Cretaceous volcanics
Metamorphic rocks
Paleozoic
Hayachine-Miyamori ofiolites
Cambrian-Ordovician

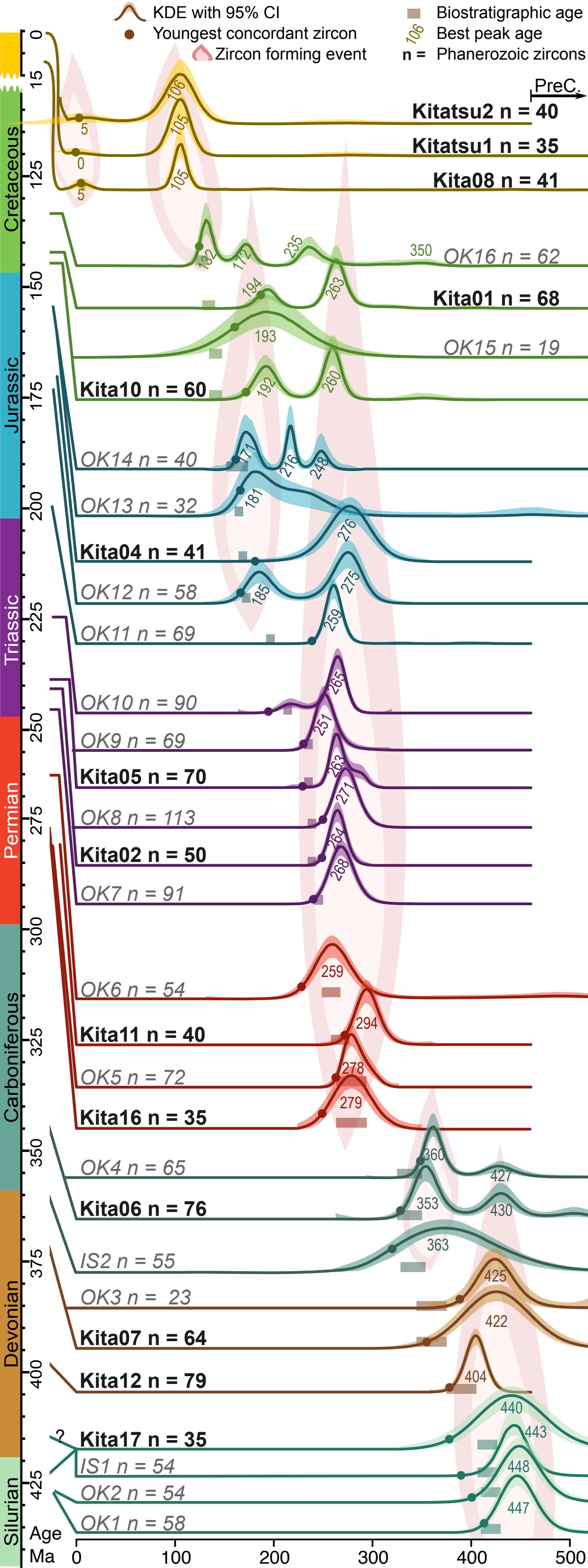

KDE with 95% CI
Youngest concordant zircon
Zircon forming event
Biostratigraphic age
106 Best peak age
n = Phanerozoic zircons
PreC.
Kitatsu2 n = 40
Kitatsu1 n = 35
Kita08 n = 41
OK16 n = 62
Kita01 n = 68
OK15 n = 19
Kita10 n = 60
OK14 n = 40
OK13 n = 32
Kita04 n = 41
OK12 n = 58
OK11 n = 69
OK10 n = 90
OK9 n = 69
Kita05 n = 70
OK8 n = 113
Kita02 n = 50
OK7 n = 91
OK6 n = 54
Kita11 n = 40
OK5 n = 72
Kita16 n = 35
OK4 n = 65
Kita06 n = 76
IS2 n = 55
OK3 n = 23
Kita07 n = 64
Kita12 n = 79
Kita17 n = 35
IS1 n = 54
OK2 n = 54
OK1 n = 58
Cretaceous
Jurassic
Triassic
Permian
Carboniferous
Devonian
Silurian
Age
Ma

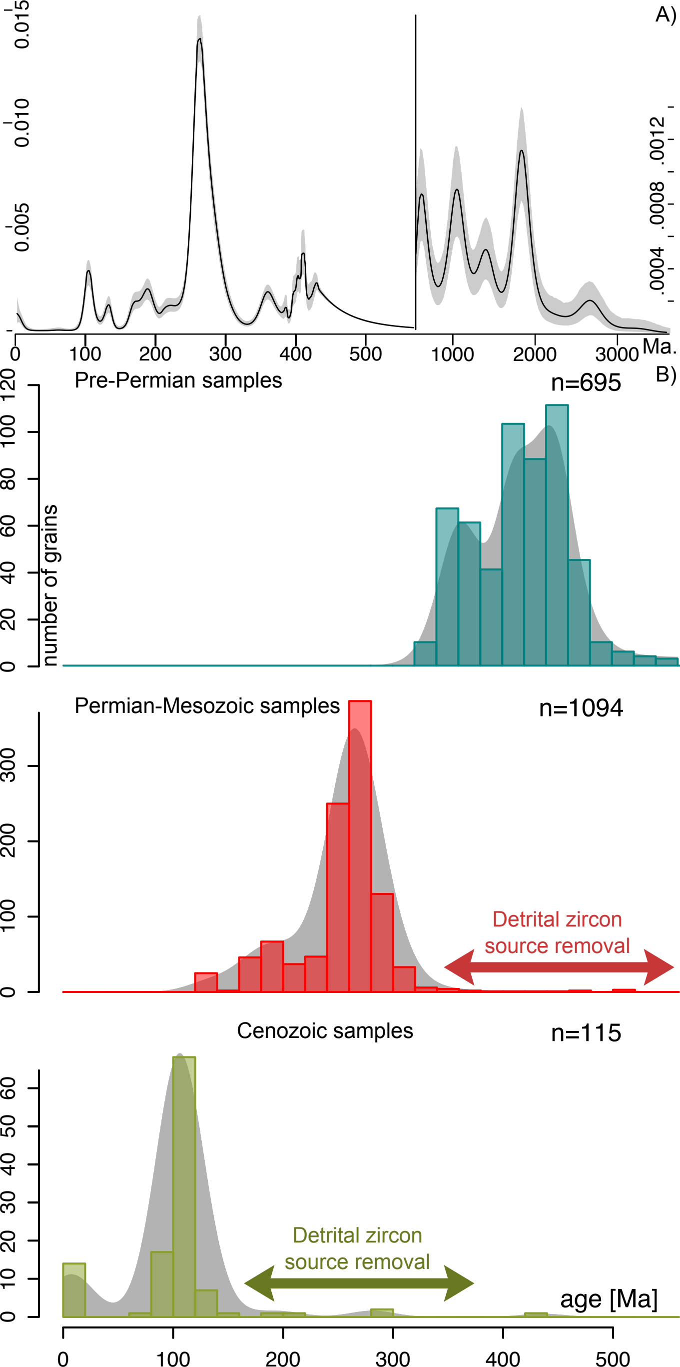
A)
0.015
0.010
0.005
.0004
.0008
.0012
0
100
200
300
400
500
1000
2000
3000
Ma.
B)
Pre-Permian samples
n=695
number of grains
0
20
40
60
80
100
120
Permian-Mesozoic samples
n=1094
0
100
200
300
Detrital zircon
source removal
Cenozoic samples
n=115
0
10
20
30
40
50
60
Detrital zircon
source removal
age [Ma]
0
100
200
300
400
500

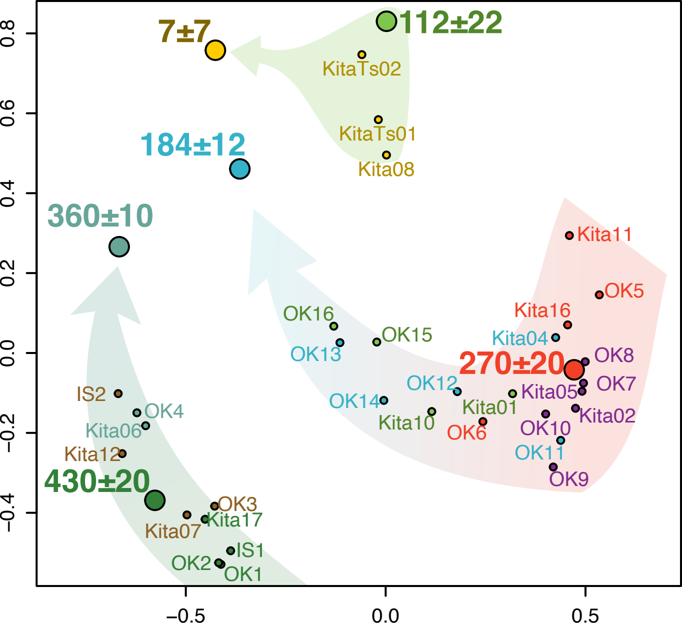
7±7
112±22
KitaTs02
KitaTs01
Kita08
184±12
360±10
Kita11
OK5
Kita16
OK16
OK15
Kita04
OK13
270±20
OK8
OK12
OK7
Kita05
OK14
Kita01
Kita02
Kita10
OK10
OK6
IS2
OK4
Kita06
Kita12
OK11
OK9
430±20
OK3
Kita17
Kita07
IS1
OK2
OK1
0.8
0.6
0.4
0.2
0.0
−0.2
−0.4
−0.5
0.0
0.5

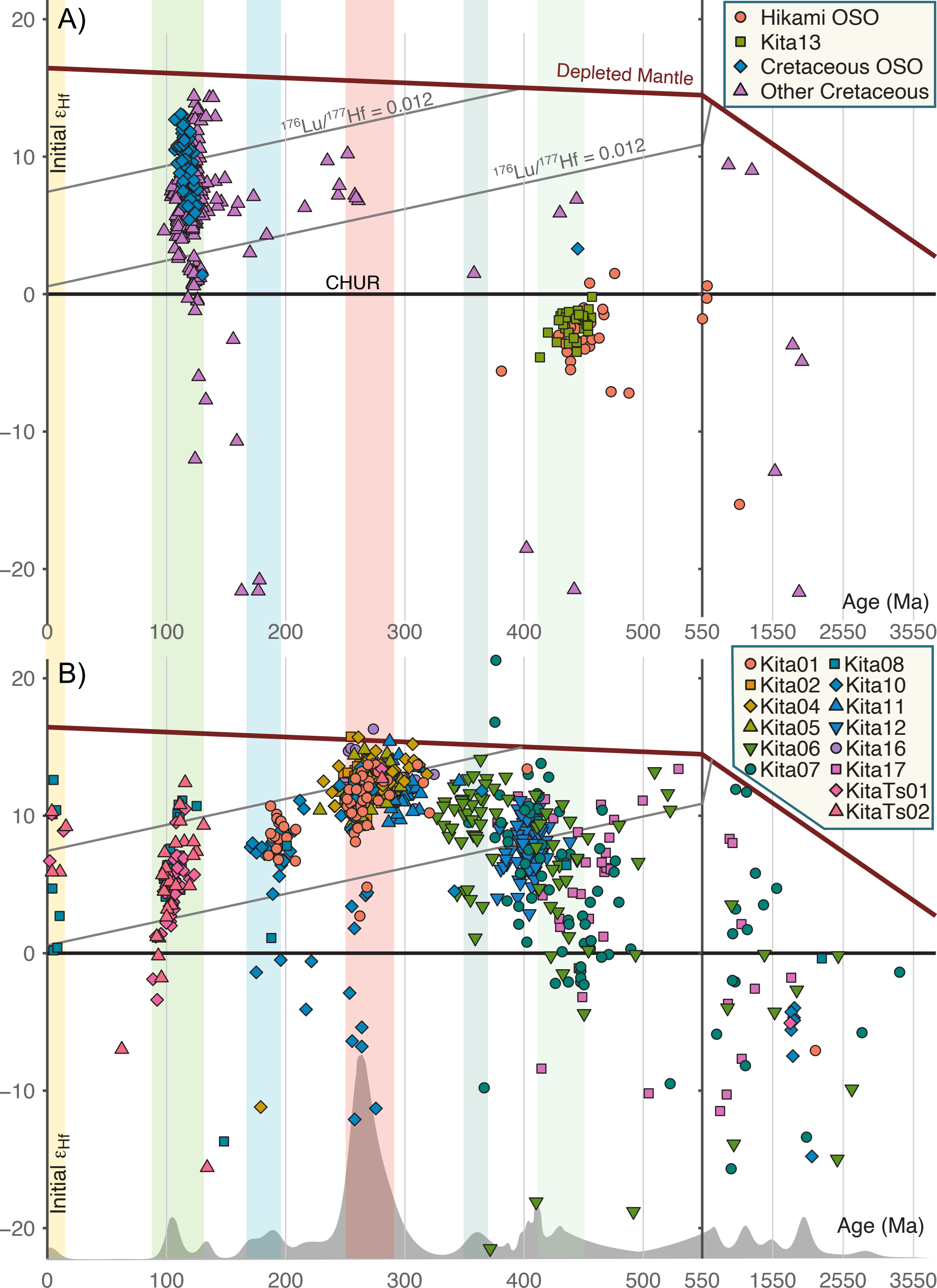

A)
Hikami OSO
Kita13
Cretaceous OSO
Other Cretaceous
Depleted Mantle
$^{176}Lu/^{177}Hf = 0.012$
$^{176}Lu/^{177}Hf = 0.012$
CHUR
Initial ε_{Hf}
Age (Ma)
B)
Kita01
Kita02
Kita04
Kita05
Kita06
Kita07
Kita08
Kita10
Kita11
Kita12
Kita16
Kita17
KitaTs01
KitaTs02
Initial ε_{Hf}
Age (Ma)

Supplementary File 1

Evidence for crustal removal, tectonic erosion and flare-ups from the Japanese evolving forearc sediment provenance

Daniel Pastor-Galán[1,2,3], Christopher J. Spencer[4,5], Tan Furukawa[3], Tatsuki Tsujimori[2,3]

[1]Frontier Research Institute for Interdisciplinary Science, Tohoku University, Japan
[2]Center for North East Asian Studies, Tohoku University, 980-8576, 41 Kawauchi, Aoba-ku, Sendai, Miyagi, Japan
[3]Department Earth Science, Tohoku University, Japan
[4]School of Earth and Planetary Sciences, The Institute for Geoscience Research (TIGeR), Curtin University, Perth, Australia
[5]Department of Geological Sciences and Geological Engineering, Queen's University, Kingston, Canada

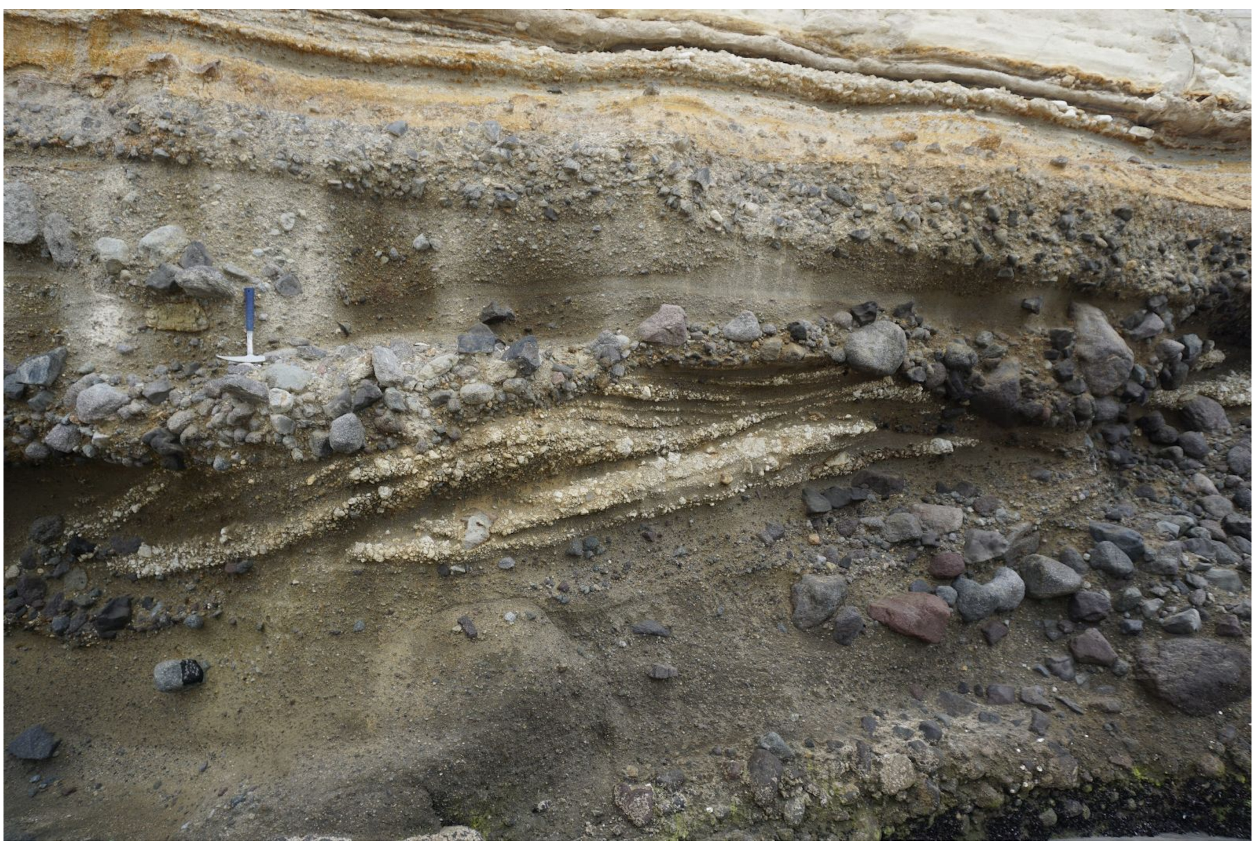

1. Site Description

Here we describe in chronological order, from older to younger, the rock formations sampled in this study (coded Kita) and those coming from the previous papers of Okawa et al. (2013) (re-coded OK) and Osozawa et al. (2019) (re-coded OSO). We provide Osozawa et al.'s (2019) samples and weighted mean ages for each pluton newly coded:

Kita 13: Ordovician-Silurian, Hikami Granite. 39.1008°, 141.6737°

The Hikami Granite is a plutonic body consisting of granites, granodiorites and tonalites. It crops out around Mt Hikami. It is usually unconformably covered by Silurian–Devonian strata. The Hikami granite has recycled zircons of 3000–1300 Ma. The Hikami granite and the Harachiyama volcanics contain chlorite and other secondary minerals, reflecting hydrothermal alteration (Osozawa et al., 2019).

OSO-08: Hikami Granite. 39.1023°, 141.6852°

KTKM-19 wt. mean of most concentrated part = 449.2±4.5 Ma (2σ)
KTKM-20 wt. mean of most concentrated part by grains which Th or U concentration is under 1,000 ppm = 442.4 ± 9.8 Ma (2σ)
BJ-13-107 wt. mean of most concentrated part = 124.9 ± 1.2 Ma (2σ) (Possibly hydrotermally altered, Osozawa et al., 2019)

OK1: Silurian. Nameirizawa Fm. 39.5488°, 141.3389°

OK2: Silurian. Yakushigawa Fm. 39.5352°, 141.6251°

Both formations are equivalent. They start with a tuff and basalts followed by mudstone and sandstone. They contain early Silurian brachiopods (Ehiro et al., 2016).

Kita 17: Silurian (?), Orikabetōge Fm. 39.5246˚, 141.3392˚

The Orikabetōge Formation is composed of conglomerates, arkoses and mudstones with subordinate amounts of limestone and tuff, and a rich fauna of Silurian corals and trilobites (Okami et al. 1986). The conglomerate contains many granitic clasts lithologically similar to Hikami granite.

IS-01 : Silurian (?), Orikabetōge Fm. 39.5286˚, 141.3855˚

Kita 12: Devonian, Ohno Fm. 39.1024°, 141.6727°

The Ono Formation is divided into the Oh1, Oh2 and Oh3 members (Minato et al. 1979). The Oh1 Member, which has yielded Pridolian radiolarians (Umeda 1996), is a slump bed which incorporates variously sized clasts of granite, arkose and limestone in a tuffaceous and siliceous mudstone. These clasts are lithologically similar to the underlying Hikami Granite and basal arkose and limestone of the Kawauchi Formation, respectively. The Oh2 Member is composed of acidic tuff and alternating beds of acidic tuff and tuffaceous-siliceous mudstone, and the Oh3 Member similarly consists mainly of tuff with subordinates amount of tuffaceous sandstone and mudstone. We sampled the top section of the formation, with an estimated age of Early-Middle Devonian

Kita 07: Devonian, Tobigamori Fm. 39.0452°, 141.2509°

The Tobigamori Formation unconformably overlies the Motai metamorphic complex. It consists of a succession of alternating thick packages of mudstones and thin sandstone beds, with purple tuffs and tuff breccias interbedded in the middle part with a total thickness of ~1000m. Its biostratigraphic age is Famenian (Ehiro and Takaizumi, 1992).

OK3: Devonian. Tobigamori Fm. 39.0672°, 141.2436°

IS-02: Carboniferous, Hikoroichi Fm. 39.1297°, 141.6611°

The Hikoroichi Formation confomarbly overlies the Devonian sequence and consists of sandstone and limestone. It contains corals, brachiopods and trilobites, and its lower-middle part and upper part are dated as Tournaisian-lower Visean and upper Visean, respectively (Ehiro et al., 2016)

Kita 06: Carboniferous, Karaumedate Fm. 39.0069°, 141.266°

Karaumedate formation conformably overlies the Tobigamori Fm. Its depositional age is late Visean. It has very variable thicknesses and it is composed of sandstones and tuffs (Eihiro and Takazumi, 1992)

OK4: Carboniferous. Karaumedate Fm. 39.007°, 141.2659°

Kita 16: Permian, Uchikawame Fm. 39.5246°, 141.2887°

The Uchikawame Formation is an Early to Middle Permian clastic formation with a thickness between 500 and 1500m. It is composed of mudstones intercalated with thin sandstone and conglomerate beds and lenses (Okami et al., 1986)

OK5: Permian. Nishikori Fm. 38.6873°, 141.2901°

It consists of sandstones and mudstones interbeded with minor limestone beds. Its age is Early Permian (Ehiro et al., 2016)

Kita 11: Permian, Hoso Fm. 38.9942°, 141.5122°

The Hosoo Formation is dominated by mudstone, and its upper and uppermost parts yield Roadian and Wordian ammonoids, respectively (Ehiro & Misaki 2005).

OK6: Permian Toyoma Fm. 38.8006°, 141.5511°

A mudstone with minor intercapations of sandstone. Tha age is Late Permian based on Wuchiapingian ammonoids (Ehiro et al., 2016).

OK7: Triassic. Osawa Fm. 38.5324°, 141.5340°

The Triassic rocks unconformably overlie the Paleozoic sequences. The Osawa Formation is composed mainly by calcareous and massive mudstones. It contains minor sandstone and conglomeratic lenses. Its age is Olenkian (Early Triassic).

Kita 02: Triassic, Fukkoshi Fm. 38.4426°, 141.4641°

The Fukkoshi Formation consists of sandstones and mudstones of Anisian age (Ehiro et al., 2016).

OK8: Triassic. Fukkoshi Fm. 38.7579°, 141.5275°

Kita 05: Triassic, Isatomae Fm. 38.4015°, 141.3683°

The Isatomae Formation lies over the Fukkoshi formation and shows a similar bio-stratigraphic Anisian age. Its 1500 m of thickness consists of silts and mudstones intercalated with thick sandstone beds (Ehiro et al., 2016).

OK9: Triassic. Isatomae Fm. 38.7134°, 141.5239°

OK10: Triassic. Shindate Fm. 38.7092°, 141.5101°

The Shindate Formation lies unconformable over the Isatomae Formation. It is composed of thick sandstones and minor mudstone and rare organic rich mudstone. Its age is Carnian (Okawa et al., 2013).

OK11: Jurassic. Niranohama Fm. 38.6931°, 141.5013°

The Niranohama Formation rests unconformably on the Triassic sedimentary sequences. It consists of sandstone and sandy mudstone and contains Hettangian (earliest Jurassic) ammonoids.

OK12: Jurassic. Aratozaki Fm. 38.6962°, 141.4985°

Unconformably over the Triassic strata, the Aratozaki formation is an arkose with conglomerate and minor mudstone. Its biostratigraphic age is Aalenian (Middle Jurassic) (Ehiro et al., 2016).

Kita 04: Jurassic, Tsukinoura Fm. 38.3816°, 141.4286°

Unconformably overlying the Isatomae formation, the Tsukinoura Formation starts with a conglomeratic and sandstone section in its lower part and continues with a monotonous thick mudstone package. The lower part yields Bajocian ammonoids (Ehiro et al., 2016)

OK13: Jurassic. Sodenohama Fm. 38.6730°, 141.4681°

Conformably over previous Jurassic strata, it consists of sandstones and mudstones with an Oxfordian–Kimmeridgian ammonoid biostratigraphic (based on Ammonoids). Ehiro et al., 2016).

OK14: Jurassic. Oginohama Fm. 38.3045°, 141.4972°

Conformably covering the previous Jurassic strata, it is composed of sandstone with intercalated mudstone and conglomerate. It contains Oxfordian–Tithonian ammonoids (Ehiro et al., 2016)

Kita 10: Cretaceous, Yoshihama Fm. 38.5768°, 141.4534°

It is a quartzitic member of the Jusanhama Group. The group unconformably covers the Jurassic strata Nagao Formation and is mainly composed of massive or bedded, quartzose or arkosic sandstones with intercalated mudstones. Biostratigraphic constraints are uncertain. Given its stratigraphic position above the Nagao Formation, the Jusanhama Group is considered to be Early Cretaceous in age (Ehiro et al., 2016).

OK15: Cretaceous. Yoshihama Fm. 38.5737°, 141.4480°

Kita 01: Cretaceous, Kanayama fm. 38.4387°, 141.3771°

This is an informal member from a small outcrop of sandstones and tufts that overlies the uppermost Jurassic Strata. It is located in the outskirts of Ichinoseki. The sample was taken in a quarry.

OK16: Cretaceous. Ayukawa Fm. 38.2916°, 141.5102°

The Ayukawa Formation conformably covers the Oginohama Formation, consists of arkose and mudstone with rare conglomerate. It contains Early Cretaceous ammonoids.

Cretacous, Kitakami Intrusives

Intrusive plutons of the southern Kitakami zone are generally granitoids with adakitic characteristics, usually associated by smaller gabbroid bodies (Osozawa et al., 2019). Chemically, the Cretaceous igneous rocks of South Kitakami Massif are varied representing a diversity of rock types: from gabbro to syenogranite, from calc-alkalic to calcic. Most of them are magnesian I type graniteoids

We have selected from Osozawa et al. (2019) the U-Pb, Lu-Hf and Sm-Nd data pertaining the plutons of south Kitakami massif:

OSO-01: Cretaceous. Tono Pluton

Tono shows a an adakitic REE pattern with a positive Eu anomaly especially in its central silicic part (Osozawa et al., 2019).
KTKM-04 wt. mean = 118.0±1.2 Ma (2σ)
This sample includes Lu-Hf

OSO-02: Cretaceous. Hitokabe Pluton

Hitokabe has an adatakitic composition.
KTKM-23 wt. mean = 114.4±1.1 Ma (2σ)

OSO-03: Cretaceous. Goyosan Pluton

KTKM-18 wt. mean = 121.7 ± 1.0 Ma (2σ)
KTKM-27 wt. mean = 120.0±2.0 Ma (2σ)
KTKM-28 wt. mean = 125.5±2.4 Ma (2σ)

OSO-04: Cretaceous. Hondera Pluton

KTKM-05 wt. mean = 113.1±1.2 Ma (2σ)

OSO-05: Cretaceous. Orikabe Pluton

This pluton shows a shoshonitic composition.

KTKM-25 wt. mean = 111.5±2.8 Ma (2σ)
KTKM-26 wt. mean = 119.0±1.9 Ma (2σ)

OSO-06: Cretaceous. Kesengawa Pluton

KTKM-21 wt. mean of most concentrated part = 122.1±1.3 Ma (2σ)

OSO-07: Cretaceous. Hirota Pluton

KTKM-22 wt. mean = 121.8±1.1 Ma (2σ)

Kita 08: Miocene, Tatsunokuchi Fm. 39.0448°, 141.2506°

The tatsunokuchi formation consists of sandstones, mudstones and tuffs. The Tatsunokuchi Formation is mainly composed of tidal flat and estuarine deposits (Yoshida et al., 2017).

Kita Tsu: Present Day, Arahama Beach, 38.2185°, 140.9866°

We sampled two differently coloured strata (dark grey and brown in the photo) from Arahama Beach, near Sendai.

2. Extra Figures

Kita 13: Ordovician-Silurian, Hikami Granite. 39.1008°, 141.6737°

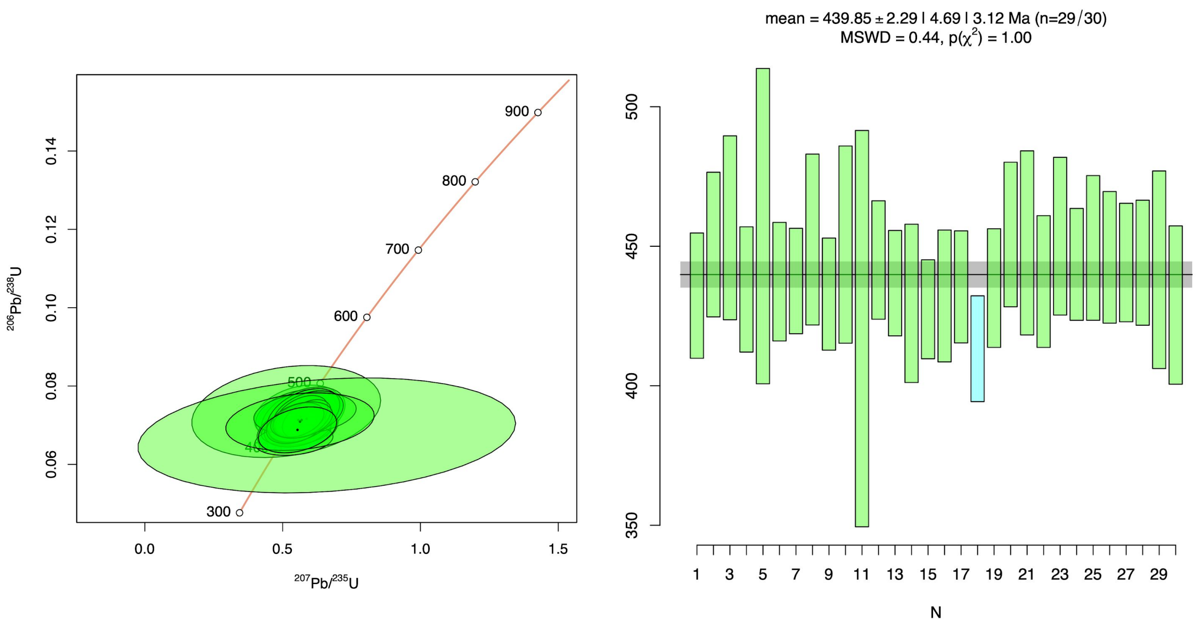

Concordia diagram (left) and mean age for the Kita 13 sample.

Map of the granitoids of Japan

Distribution of granitoids in Japan. The location of the South Kitakami mountains is marked.

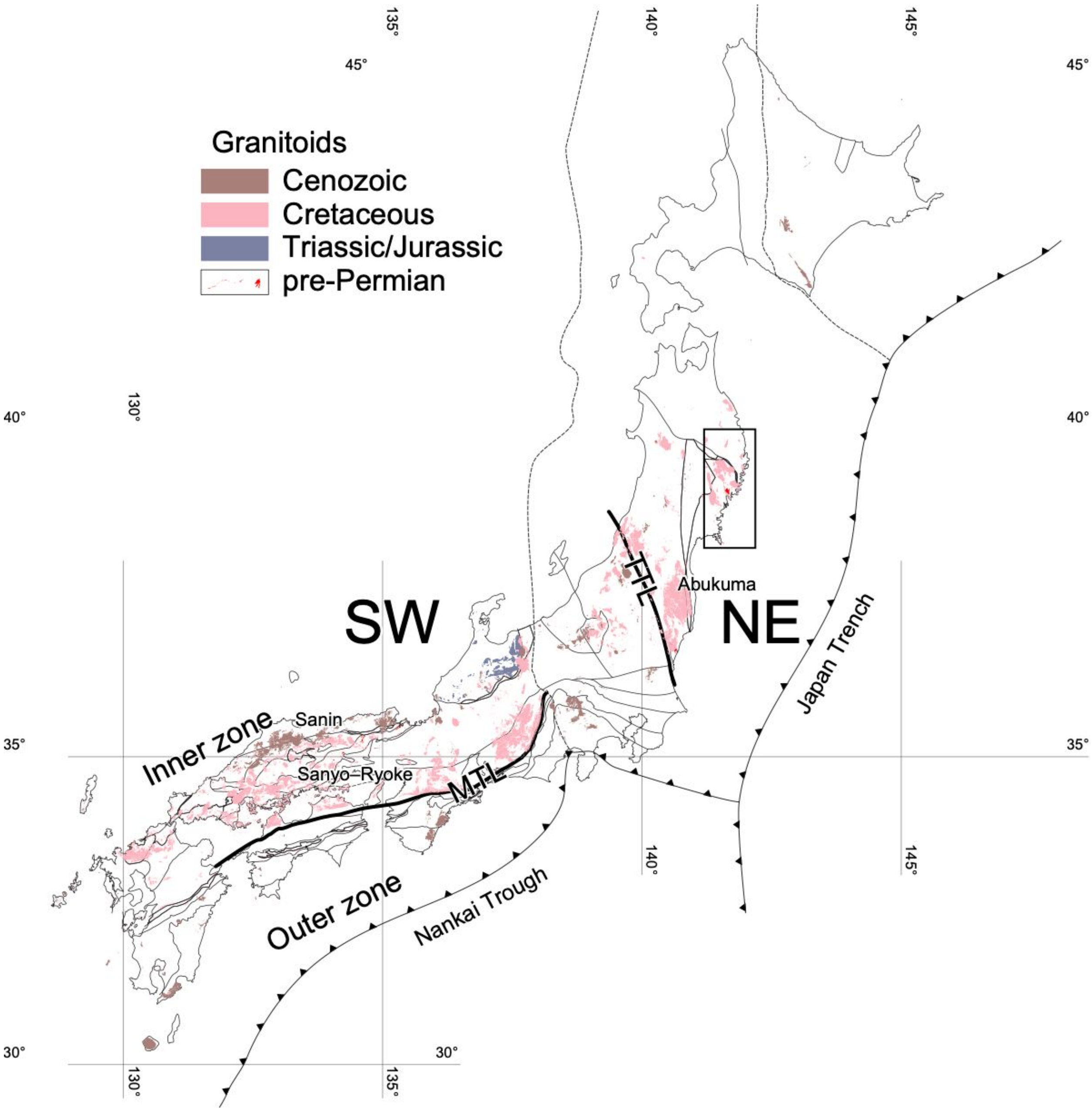

3. BAD-ZUPA

BAD-ZUPA (Bayesian Approach for Detrital Zircon U-Pb ages) is a new evaluation protocol based on Riihimaki and Vehtari (2014)'s Laplace approximation with logistic Gaussian process regression (LA-LGP). BAD-ZUPA evaluates the probability density function (PDF) and their integration, the cumulative distribution function (CDF) through two algorithms: (I) confidence interval estimation and (II) peaks estimation. With BAD-ZUPA, we can evaluate the confidence we have on a detrital zircon spectrum and the significance of the observed peaks. In addition, BAD-ZUPA is a powerful tool to estimate how many more zircons we would need to analyze to obtain a desired level of confidence.

The code is citable though the DOI:

10.5281/zenodo.4138657

The code and a short description and a user manual is available in:

https://github.com/Tan-Furukawa/badzupa

https://rdrr.io/github/Tan-Furukawa/badzupa/

4. Zircon standards used

The primary reference material analyzed for U–Pb dating in this study was 91500 (1,062.4 ± 0.4 Ma in Wiedenbeck et al. (1995) with GJ1 (601.92 ± 0.7 Ma in Jackson et al., 2004) as a secondary age standard. During the two analytical sessions, 91500 yielded a $^{206}Pb/^{238}U$ weighted average age of 1,062 ± 3 Ma (MSWD = 3.6, n = 61; self-normalized) and 1062 ± 2 Ma (MSWD = 0.9, n = 39). GJ1 yielded a $^{206}Pb/^{238}U$ weighted average age of 603 ± 2 Ma (MSWD = 13.5, n = 62) and 601 ± 2 Ma (MSWD = 5.1, n = 40). Ages calculated for the secondary standards, treated as unknowns, were found to be within 1% of the accepted value. The time-resolved mass spectra were reduced using the U_Pb_Geochronology3 data reduction scheme in Iolite (Paton et al., 2011).

Reference zircon Mudtank (0.282507 ± 0.000008 in Fisheret al., 2014) was used to monitor accuracy and precision of internally corrected (using $^{179}Hf/^{177}Hf$ = 0.7325) Hf isotope ratios (Woodhead & Hergt, 2005). 91500 (0.282306 ± 0.000008) and GJ1 (0.282000 ± 0.000005 in Morel et al., 2008) were used as secondary standards. During the analytical sessions, Mudtank yielded a corrected $^{176}Hf/^{177}Hf$ weighted average ratio of 0.282507 ± 0.000006 (MSWD = 1.1, n = 62; self-normalized) and 02.28507 ± 0.000006 (MSWD = 1.0, n = 42). 91500 yielded a corrected $^{176}Hf/^{177}Hf$ weighted average ratio of 0.282307 ± 0.000012 (MSWD = 2.2, n = 61) and 0.282296 ± 0.000008 (MSWD = 1.5, n = 42). GJ1 yielded a corrected 176Hf/177Hf weighted average ratio of 0.282022 ± 0.000010 (MSWD = 2.0, n = 62) and 0.282011 ± 0.000008 (MSWD = 1.7, n = 42). All of the corrected values of secondary standards are within 0.01% of the correct value. The stable $^{178}Hf/^{177}Hf$ and $^{180}Hf/^{177}Hf$ ratios for the reference materials yielded values of 1.46726 ± 0.000008 and 1.88690 ± 0.00007, respectively, and are within 200 ppm of known values based upon atomic masses and abundances (Spencer et al., 2020). Reproducibility of the $^{78}Hf/^{177}Hf$ and $^{180}Hf/^{177}Hf$ ratios are, respectively, 113 and 85 ppm.

5. References

Ehiro, M., Tsujimori, T., Tsukada, K., & Nuramkhaan, M. (2016). Palaeozoic basement and associated cover. In T. Moreno, S. R. Wallis, T. Kojima, & W. Gibbons (Eds.), The geology of Japan (pp. 25–60). London, England: The Geological Society of London.

Ehiro, M., and Takaizumi, Y., 1992, Late Devonian and Early Carboniferous ammonoids from the Tobigamori Formation in the Kitakami Massif, Northeast Japan and their stratigraphic significance, Jour. Geol. Soc. Japan vol. 98, p. 197-204

Fisher, C.M., Vervoort, J.D., Hanchar, J.M., 2014. Guidelines for reporting zircon Hf isotopic data by LA-MC-ICPMS and potential pitfalls in the interpretation of these data. Chemical Geology 363, 125–133. https://doi.org/10.1016/j.chemgeo.2013.10.019

Jackson, S.E., Pearson, N.J., Griffin, W.L., Belousova, E.A., 2004. The application of laser ablation-inductively coupled plasma-mass spectrometry to in situ U–Pb zircon geochronology. Chemical Geology 211, 47–69. https://doi.org/10.1016/j.chemgeo.2004.06.017

Minato, M., Kato, M., Haga, S., 1979, Stratigraphy, Silurian. In Minato, M., Hunahashi, M., Watanabe, J. and Kato, M ends., The Abean Orogeny, Tokai Univ. Press, 56-59

Misaki, A., and Ehiro, M., 2004, Stratigraphy and geologic age of the Middle Permian in the Kamiyasse-Imo district, Southern Kitakami Massif, Northeast Japan, Jour. Geol. Japan, Vol.110, p. 129-145

Okami, K., Ehiro, M., Oishi, M., 1986, Geology of the Lower-Middle Paleozoic around the northern marginal part of the Southern Kitakami Massif, with reference to the geologic development of “Hayachine Tectonic Belt”, 北村信教授記念地質論文集, p.313-330

Okawa, H., Shimojo, M., Orihashi, Y., Yamamoto, K., Hirata, T., Sano, S.I., Ishizaki, Y., Kouchi, Y., Yanai, S. and Otoh, S., 2013. Detrital zircon geochronology of the Silurian–Lower Cretaceous continuous succession of the South Kitakami belt, northeast Japan. Memoir of the Fukui Prefectural Dinosaur Museum, 12, pp.35-78.

Osozawa, S., Usuki, T., Usuki, M., Wakabayashi, J. and Jahn, B.M., 2019. Trace elemental and Sr-Nd-Hf isotopic compositions, and U-Pb ages for the Kitakami adakitic plutons: Insights into interactions with the early Cretaceous TRT triple junction offshore Japan. Journal of Asian Earth Sciences, 184, p.103968.

Paton, C., Hellstrom, J., Paul, B., Woodhead, J., Hergt, J., 2011. Iolite: Freeware for the visualisation and processing of mass spectrometric data. J. Anal. At. Spectrom. 26, 2508–2518. https://doi.org/10.1039/C1JA10172B

Riihimäki, J. and Vehtari, A., 2014. Laplace approximation for logistic Gaussian process density estimation and regression. Bayesian analysis, 9(2), pp.425-448.

Spencer, C.J., Kirkland, C.L., Roberts, N.M.W., Evans, N.J., Liebmann, J., 2020. Strategies towards robust interpretations of in situ zircon Lu–Hf isotope analyses. Geoscience Frontiers 11, 843–853. https://doi.org/10.1016/j.gsf.2019.09.004

Umeda, M., 1996, Radiolarian fossils from the Devonian Onoand Nakazato Formations in the southern Kitakami Belt, Northeast Japan, Earth Science (Chikyu Kagaku), 50, p.311-336

Wiedenbeck, M., Allé, P., Corfu, F., Griffin, W.L., Meier, M., Oberli, F., Quadt, A.V., Roddick, J.C., Spiegel, W., 1995. Three Natural Zircon Standards for U-Th-Pb, Lu-Hf, Trace Element and Ree Analyses. Geostandards Newsletter 19, 1–23. https://doi.org/10.1111/j.1751-908X.1995.tb00147.x

Yoshida, M., Hoyanagi, K., Kondo, H., Inoue, H., Oishi, M., Yoshida, H. and Yanagisawa, Y., 2007. Sequence stratigraphy and organic matter preservation of the Miocene to Pliocene Tatsunokuchi Formation, Iwate, Northeast Japan. Journal of the Sedimentological Society of Japan, 64, pp.21-26.